



**CHALMERS**  
UNIVERSITY OF TECHNOLOGY

---



# **CFD simulation and Experimental Study of a Carbon Canister**

Master's thesis in Master Programme Sustainable Energy Systems

Muhammad Hassan Zafar



THESIS FOR DEGREE OF MASTER OF SCIENCE

# CFD simulation and Experimental Study of a Carbon Canister

Muhammad Hassan Zafar



**CHALMERS**  
UNIVERSITY OF TECHNOLOGY

Master's Programme in Sustainable Energy Systems  
*Master's Thesis Registered at Department of Chemistry and Chemical Engineering*  
CHALMERS UNIVERSITY OF TECHNOLOGY  
Gothenburg, Sweden 2019

CFD simulation and Experimental Study of a Carbon Canister  
Muhammad Hassan Zafar

© Muhammad Hassan Zafar, 2019.

Master Thesis conducted at Volvo Cars Corporation (VCC), Fuel Systems Department.

Supervisors at VCC: Göran Fredriksson, Ehsan Yasari & Robert Palm  
Examiner: Derek Creaser, Department of Chemistry and Chemical Engineering

Master's Programme in Sustainable Energy Systems  
Master's Thesis Registered at Department of Chemistry and Chemical Engineering  
Chalmers University of Technology  
SE-412 96 Gothenburg  
Telephone +46 31 772 1000

## Abstract

The release of Volatile Organic Compounds (VOCs) from the fuel storage system in vehicles into the atmosphere poses a serious threat to both health of living organisms and plants. To capture these evaporative emissions, the carbon canister is installed. The canister has a bed of activated carbon which adsorbs the incoming VOCs from fuel tank and prevents their escape into the atmosphere. These adsorbed hydrocarbons are then purged by establishing a flow of air through the canister and the desorbed volatiles are sent to the engine for energy recovery.

This study focuses on the development of both 1D and 3D simulation models of carbon canisters. A major part of this project was related to the experimental work that was performed on two fabricated canisters. The experiments were carried out for loading, purging, purge gas heating and carbon bed insulation cases. The experimental results were obtained in the form of mass gain, temperature profiles and concentration measurements. These results were used to calibrate the simulation models and compare the results.

The adsorption phenomena was incorporated into the simulation models by implementation of adsorption model. The Linear driving Force (LDF) model was used to define the rate of adsorption. The Dubinin Astakhov isotherm was used to describe the equilibrium adsorption of n-Butane on activated carbon. This model was implemented both in GT-SUITE for 1D modelling and STAR-CCM+ for 3D modelling.

There was a varying degree of accuracy for both the 1D and 3D model compared to the experimental results. The 1D model was able to predict the mass change of canister very well but greatly over estimated the temperatures inside the bed. On the other hand, the 3D model was not able to predict accurate breakthrough time with breakthrough occurring earlier in comparison to experiments. The temperature profiles however showed better agreement with experimental data than the 1D model. The purge gas heating simulations showed that the model was underestimating the mass loss of the canister in comparison to the experimental data. A comparison of results for insulated and uninsulated canister is also shown. Finally, the effect of change in altitude is shown on the canister loading.

The 3D model showed promise since it provided better results and additional details than the 1D model. It is also concluded that the calibration is of prime importance with the tuning parameters varying for each 1D, 2D and 3D simulation cases. The 3D model needs further calibration to accurately predict the mass change and temperature profiles. The experimental procedure for concentration measurement was found to have high degree of error and hence no good comparison was achieved with the simulation results.

Keywords: Carbon canister, Linear Driving Force (LDF), Dubinin Astakhov isotherm, GT-Suite, STAR-CCM+.



## Acknowledgements

This thesis was carried out at Volvo Cars Corporation and was made possible by the assistance of several people. First of all I would like to thank my supervisors Göran Fredriksson, Ehsan Yasari and Robert Palm for their continuous support, guidance and feedback throughout the course of the project. I would especially like to mention Anders Aronsson without whom the experimental setup would not have been possible. I would also like to thank my examiner, Derek Creaser, for his feedback on my report drafts.

I would like to thank Meisam Farzaneh at Volvo Cars for his assistance regarding software related issues throughout the project. I am very grateful to Michael Heim at Ingevity who provided me with valuable data. I would also like to appreciate the assistance provided by Ludvig Uppstroem, Jeremy Dahan and Thomas Eppinger at Siemens for setting up the 3D model in Star-CCM+.

Huge thanks to my fellow thesis workers, especially Oscar Sundell and Jakob Dahlqvist who assisted me with my experiments.



# Contents

<b>List of Figures</b>	<b>xi</b>
<b>List of Tables</b>	<b>xiii</b>
<b>1 Introduction</b>	<b>1</b>
1.1 Background . . . . .	1
1.2 Thesis objective . . . . .	3
1.3 Demarcation . . . . .	3
1.4 Approach . . . . .	3
<b>2 Theory</b>	<b>5</b>
2.1 Working of a Carbon canister . . . . .	5
2.2 Adsorption . . . . .	7
2.2.1 Working principle . . . . .	7
2.2.2 Kinetics and equilibrium . . . . .	8
2.2.2.1 Dubinin Astakhov Isotherm . . . . .	8
2.2.2.2 Isosteric heat of adsorption . . . . .	9
2.2.3 Linear Driving Force (LDF) model . . . . .	9
2.2.4 LDF model using Dubinin Astakhov isotherm . . . . .	10
2.2.5 Activated carbon as adsorbent . . . . .	11
2.3 Computational Fluid Dynamics (CFD) . . . . .	12
2.3.1 1D/2D modelling in GT Suite . . . . .	13
2.3.2 3D Modelling in Star CCM+ . . . . .	16
<b>3 Experimental and simulation method</b>	<b>19</b>
3.1 Experiments . . . . .	19
3.1.1 Setup . . . . .	19
3.1.1.1 Large canister . . . . .	19
3.1.1.1.1 Canisters geometry . . . . .	21
3.1.1.1.2 Sensors and sampling ports . . . . .	21
3.1.1.1.3 Insulation . . . . .	21
3.1.1.2 Small canister . . . . .	21
3.1.1.2.1 Canisters geometry . . . . .	22
3.1.1.2.2 Sensors and sampling ports . . . . .	23
3.1.1.3 Canister length to diameter (L/D) ratio . . . . .	24
3.1.1.4 Entrance length . . . . .	24
3.1.1.5 Canister cycling . . . . .	25

3.1.2	Tests . . . . .	25
3.1.2.1	Pressure drop . . . . .	25
3.1.2.2	Loading . . . . .	26
3.1.2.3	Idle time . . . . .	27
3.1.2.4	Purging . . . . .	28
3.1.2.5	Purge flow heating . . . . .	28
3.1.2.6	Gas sampling . . . . .	29
3.2	Simulations . . . . .	29
3.2.1	GT Suite . . . . .	30
3.2.1.1	Simulation Model . . . . .	30
3.2.1.2	Numerical setup . . . . .	33
3.2.1.3	Implementation of adsorption model . . . . .	34
3.2.1.4	Calibration . . . . .	35
3.2.1.5	Simulation cases . . . . .	35
3.2.1.5.1	Pressure drop . . . . .	35
3.2.1.5.2	Loading . . . . .	36
3.2.1.5.3	Purging . . . . .	36
3.2.1.5.4	Purge gas heating . . . . .	36
3.2.1.5.5	Altitude . . . . .	36
3.2.2	Star CCM+ . . . . .	37
3.2.2.1	Geometry construction . . . . .	37
3.2.2.2	3D model setup . . . . .	37
3.2.2.2.1	Pressure drop . . . . .	40
3.2.2.2.2	Adsorption model . . . . .	40
3.2.2.2.3	Calibration . . . . .	41
<b>4</b>	<b>Results and discussion</b>	<b>43</b>
4.1	Pressure drop . . . . .	43
4.2	Loading . . . . .	45
4.2.1	Small canister . . . . .	45
4.2.2	Large canister (Without insulation) . . . . .	48
4.3	Purging . . . . .	48
4.3.1	Small canister . . . . .	48
4.3.2	Large canister (Without insulation) . . . . .	51
4.4	Simulation results . . . . .	51
4.4.1	Butane Storage (Loading) . . . . .	51
4.4.2	Temperature profiles . . . . .	53
4.4.3	Purge gas heating . . . . .	54
4.4.4	Altitude variation . . . . .	55
4.5	Canister Insulation . . . . .	56
4.6	Concentration profiles . . . . .	59
<b>5</b>	<b>Conclusion</b>	<b>63</b>
<b>6</b>	<b>Future work</b>	<b>65</b>
	<b>Bibliography</b>	<b>67</b>

# List of Figures

1.1	World wide emission legislation for passenger cars Forecast 2020+ [1].	2
2.1	Dual channel carbon canister.	5
2.2	Loading (left) and purging (right) flow inside the carbon canister.	6
2.3	Difference between adsorption and absorption.	7
2.4	Isotherm fitting at temperature of 25° C (left) and 100° C (right)	11
3.1	The large experimental canister.	20
3.2	Large canister dimensions	20
3.3	Large canister sensors and sampling ports positions	22
3.4	The small fabricated canister.	22
3.5	Small canister dimensions	23
3.6	Small canister sensors and sampling ports positions	24
3.7	Mass change during cycling of small canister (left) and large canister (right).	25
3.8	Position of pressure ports on the canister for pressure measurement.	26
3.9	Experimental setup for loading of canister.	27
3.10	Schematic for the experimental setup during loading of canister.	28
3.11	Experimental setup for purging of canister.	29
3.12	1D model layout in GT-SUITE. The template titles in GT-SUITE are shown in brackets ().	30
3.13	Discretization length representation for carbon bed in 1D and 2D.	34
3.14	Inlet temperatures during purge gas heating experiments.	37
3.15	Small canister geometry as made in ANSA pre processor.	38
3.16	Small canister geometry as made in ANSA pre processor.	39
4.1	Pressure drop across the small canister (left) and large canister (right).	44
4.2	Comparison of pressure drop obtained by experiment and simulation across the carbon bed in small canister (left) and large canister (right)	44
4.3	Mass change during loading of small canister.	46
4.4	Temperature change during loading of small canister at four axial positions. For each axial position, the temperature at three radial positions are plotted.	46
4.5	Mass change during loading of large canister (without insulation).	47
4.6	Temperature change during loading of large canister (without insulation) at three axial positions. The radial positions are shown as distance from the wall in each plot.	47

4.7	Mass change during purging of small canister. . . . .	49
4.8	Temperature change during purging of small canister at four axial positions. . . . .	49
4.9	Mass change during purging of large canister (without insulation). . .	50
4.10	Temperature change during purging of large canister (without insulation) at three axial positions. . . . .	50
4.11	Mass change during loading (left) and purging (right) for experiment and 1D simulation. . . . .	52
4.12	Comparison of mass change during loading between experimental and simulation results. . . . .	52
4.13	Comparison of temperature profiles obtained by 1D (left) and 3D (right) simulations for small canister loading process with inlet flowrate of 0.8 L/min (50% n-Butane and 50% Nitrogen). . . . .	53
4.14	<b>Left:</b> Comparison of mass loss during purging of small canister between simulation and experimental results. <b>Right:</b> Inlet temperatures for different cases of purge flow heating. . . . .	54
4.15	Effect of altitude variation on the n-butane storage capacity of the small canister (1D model results). . . . .	55
4.16	Mass change and temperature profiles during loading process for insulated and uninsulated canister. . . . .	57
4.17	Mass change and temperature profiles during purging process for insulated and uninsulated canister. . . . .	58
4.18	The signal data received from the automotive emission analyzer for Hydrocarbon concentration in ppmvol for the loading experiment conducted on small canister with total inlet flowrate of 0.4 L/min. . . . .	59
4.19	Loading experiment results of n-Butane concentration at 3 different radial positions inside the small canister with total inlet flowrate of 0.4 L/min. . . . .	60
4.20	3D simulation scene for butane concentration mass fraction in small canister with total inlet flowrate of 0.4 L/min. . . . .	61

# List of Tables

2.1	Parameters for n-Butane used in the Antoine equation as given by NIST. . . . .	10
2.2	Pore sizes and their properties in typical activated carbons. . . . .	12
3.1	Experimental conditions for pressure drop test for both canisters. . .	26
3.2	Initial conditions for the 1D GT-SUITE model for the loading and purging cases. . . . .	33
3.3	Tuning parameter values for 1D GT-SUITE model. . . . .	35
3.4	Tuning parameter values for 3D STAR-CCM+ model. . . . .	41
4.1	Calibration parameters for 3D model. . . . .	53
4.2	Absolute pressure observed in atmosphere at different altitudes (Values taken from GT-SUITE software). . . . .	56



# 1

## Introduction

### 1.1 Background

Ozone layer in the upper atmosphere, called Stratosphere, protects our planet from harmful ultraviolet rays. But ozone near the surface acts as the main ingredient in the formation of smog. Smog is formed by a set of complex photochemical reactions involving Volatile Organic Compounds (VOCs), nitrogen oxides (NO<sub>x</sub>) and sunlight which form ground level ozone. Smog poses serious health problems which include respiratory problems, eye infections and damage to the immune system. It also inhibits plant and forest growth which results in loss of biodiversity as well as damage to the economy. In the 1960s, serious concerns arose in the US due to deteriorating air quality in Urban settlements [2]. This led to the formation of the US Environmental Protection Agency (EPA) in the 1970. Since the tail pipe emissions from vehicles was the major source of VOCs and NO<sub>x</sub> [3].

In the 1970s EPA imposed regulations on all light duty vehicles for control of emissions. This led to development of implementation of catalytic reduction techniques for tail pipe emissions control and carbon canisters for the evaporative emission from fuel tank. Efforts to reduce tail pipe emissions have been very successful and significant reduction in VOCs and NO<sub>x</sub> have been achieved over the years. This led to renewed focus on the less obvious source of emissions i.e. the evaporative emissions from fuel tank [4].

The evaporative emissions result from the evaporation of fuel inside the fuel tank which leads to pressure build up inside the tank. This evaporation is triggered by two scenarios. Firstly, due to ambient temperature increase, the fuel inside the tank begins to vaporize and secondly, during refueling, the gas phase inside the fuel tank is compressed by the incoming liquid fuel. In a closed fuel tank, both these scenarios will lead to an increase in the fuel tank pressure. But for safety reasons, the fuel tank is not pressurized. The easiest solution is to release the build up vapor to the atmosphere. Since these vapors are made up of high concentrations of hydrocarbons (HC), they need to be captured.

To capture the compounds from these evaporative emissions, the carbon canister is installed. The carbon canister is now part of the On-board Fuel Vapor Recovery (ORVR) system which is the vehicle fuel vapor emission control system employed by the automotive industry. As years go by, the legislation for emission control

## 1. Introduction

---

have become more and more stringent. So far the vehicle manufacturers have been able to cope up with these regulations by using larger sized canisters and improved activated carbon [5].

With the rise of hybrid vehicles, the vehicle manufacturers are now faced with a new problem. In a normal car with internal combustion engine, the loaded canister is purged when the vehicle is running and the purged HCs are sent to the engine. In hybrid vehicles, the fuel tank is the same so the evaporative emission levels are the same. But problem arises due to the fact that for short travels, in hybrid vehicles, the internal combustion engine might not run at all so the canister won't be purged and eventually the canister will become saturated and start to emit HCs into the atmosphere. To control this issue, new and improved canister with improved purging mechanism is required to keep up with the increasing number of hybrid vehicles.

Figure 1.1 shows the various legislation around the world that would be implemented after 2020. The purpose of this image is to show the presence of different kinds of regulations that each country or region follows, the choice of which is completely dependant on governmental policies. So far, US has the most stringent emission control laws but with each passing year, the other regions are moving towards more strict laws as well[1].

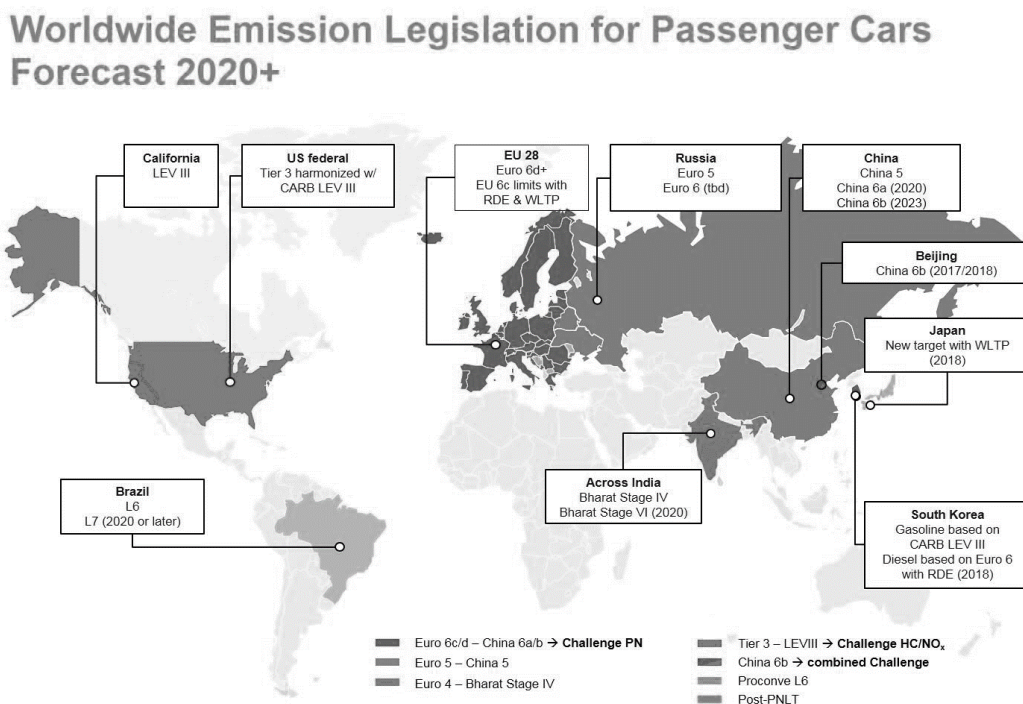


Figure 1.1: World wide emission legislation for passenger cars Forecast 2020+ [1].

## 1.2 Thesis objective

The purpose of this thesis include the following:

- Understanding the effect of radial heat transfer during adsorption and desorption.
- Investigating the butane concentration profiles in radial and axial directions during the adsorption and desorption process.
- Understanding the effect of heat addition to purge flow on the desorption process.
- Developing a 3D canister model.

## 1.3 Demarcation

The scope of this project is limited to the study of carbon canisters with cylindrical geometry and hence, the actual canister geometry is not considered. The aim of the project is to understand how the temperature and concentration profiles look like inside the canister and to produce a working 1D and 3D model that are able to capture these profiles. For the experimental study, two canisters of different dimensions were fabricated. However, for the simulations, both in 1D and 3D, the small canister geometry was simulated and the larger canister geometry was out of scope of simulations. Furthermore, for 3D model, only the loading cycle of canister, as explained later, was simulated. Also, the 3D model developed for the loading process was run with laminar flow model. Finally, for the entire study, the fuel used was n-Butane and no tests or simulations were carried out with actual fuel such as gasoline.

For the simulation models, the activated carbon pellets were assumed to be spherical. This assumption was used to simplify the simulations. In reality, the activated carbon pellets are not entirely spherical and somewhat resemble a cylindrical shape.

## 1.4 Approach

This project is divided into both experimental and simulation work. The experiments are carried out on two cylindrical canisters having different dimensions. Parameters such as mass change of canister, temperatures and concentrations inside the carbon bed were monitored during both the loading (adsorption) and purging (desorption) experiments in order to obtain the necessary data for calibration of simulation models and later comparison of model results with the experimental data.

The simulations were performed both in 1D and 3D. The 1D simulation of carbon canisters were performed in GT-SUITE v2018 developed by Gamma Technologies and 3D simulations were performed in STAR-CCM+ software developed by Siemens. MATLAB by Mathworks was used for comparison of experiment and simulation data and creation of plots.



# 2

## Theory

In this chapter, the theory behind the adsorption principle is covered briefly. An introduction to the adsorption model used is also presented along with the choice of model used in this study. The working principle of a carbon canister is discussed and the methods of modelling the canister using Computational Fluid Dynamics (CFD) are also presented.

### 2.1 Working of a Carbon canister

A carbon canister diagram is shown in figure 2.1. In simple words, the canister is just a container filled with activated carbon pellets. The canister has three connections. The tank port (1) connects the canister to the fuel tank, the purge port (2) connects the canister to the engine and the atmospheric port (3), as the name suggests, is a connection that is open to atmosphere [6].

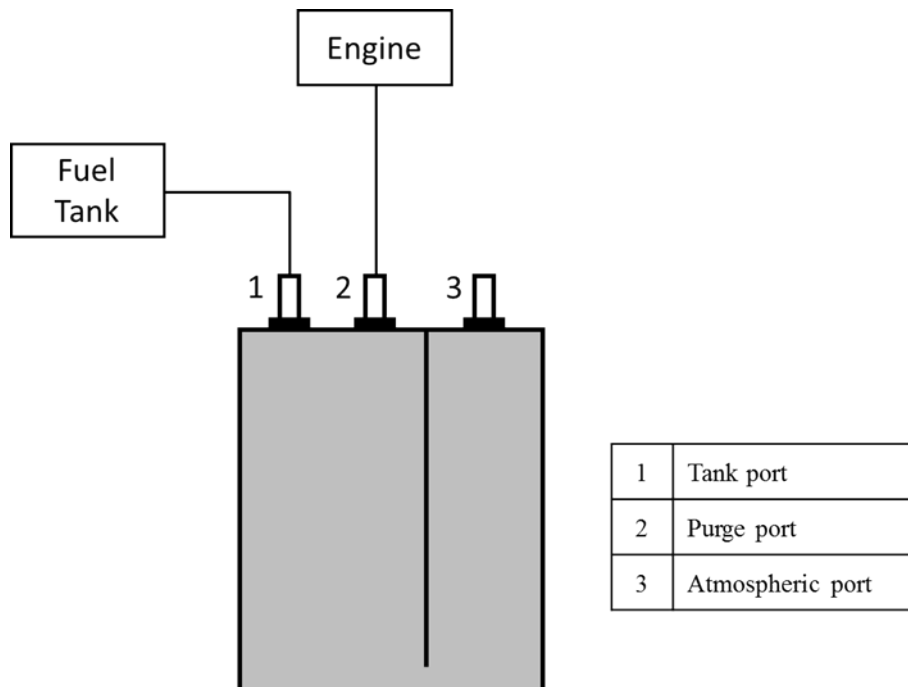


**Figure 2.1:** Dual channel carbon canister.

The canister is designed to capture all the hydrocarbon vapors that are originated in the fuel tank. As stated before, these vapors can either be formed in the fuel

tank due to temperature increase or during the refuelling process. The vapor-air mixture enter the canister via the tank port. Before coming into contact with the activated carbon, the flow passes through a foam which serves two purposes. Firstly, it helps to hold the activated carbon in place and secondly, it creates a resistance to flow so that the incoming flow through the canister is more uniform. This flow of vapors into the canister is known as the 'loading' process. As the vapors flow into the canister, the hydrocarbons are adsorbed onto the activated carbon pellets. The adsorption process, being exothermic, leads to an increase in temperature inside the activated carbon bed. Figure 2.2 (left) shows the flow direction during the loading process. During the loading process, the purge port (2) is closed so the flow moves from the tank port to the atmospheric port. Since the hydrocarbon vapors are adsorbed inside the bed, only the air exits the canister via the atmospheric port.

Since the canister has limited capacity to store the incoming hydrocarbons from the fuel tank, the activated carbon bed needs to be regenerated. This is achieved by the 'purging' process wherein a reverse flow of atmospheric air is established via the atmospheric port (3) through the canister. This air contact with the loaded carbon results in the desorption of the stored hydrocarbon and a temperature drop occurs inside the carbon bed due to the endothermic desorption. Figure 2.2 (right) shows the flow direction during the purging process. During the purging process, the tank port (1) is closed and air enters via the atmospheric port (3) and the hydrocarbon laden air leaves the canister via the purge port (2) and is sent to the engine where these hydrocarbons are burned and their energy is recovered. The driving force for this purge flow is provided by the low pressure created inside the engine, below atmospheric pressure, which establishes the air flow through the canister.

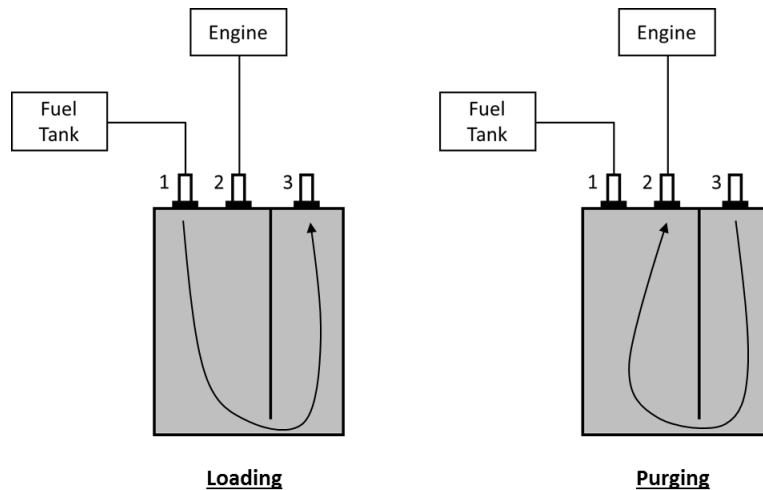


**Figure 2.2:** Loading (left) and purging (right) flow inside the carbon canister.

In figure 2.1, the dual channel geometry is shown. This configuration helps in achieving an optimum L/D ratio of the porous bed. Both the number of channels and the L/D ratio are design choices. Several studies have been conducted regarding different designs of carbon canister. Roger and Ried [7] researched the effects of varying L/D ratio using dual channel geometry and concluded that an increase in

L/D ratio from 1 to 3.5 reduced the bleed emissions from the canister. Similar results were obtained in a study performed by Zhang et al. who also stated the benefits of using a L/D ratio greater than 1 and use of double cavity design [8].

## 2.2 Adsorption

Adsorption is the process by which molecules from the bulk fluid phase move to a solid surface due to presence of physical forces or formation of a chemical bond. The adsorbing fluid and the solid surface is termed as adsorbate and adsorbents respectively [9].

### 2.2.1 Working principle

In adsorption, the molecules collect on the solid surface. These surfaces can be external surface or internal surfaces i.e. crevices inside the solid. Adsorption can also occur on a liquid surface. On the other hand, absorption refers to the movement on fluid into the solid or liquid, and unlike adsorption, where molecules only adhere to the surface, absorption results in penetration of molecules inside the solid or liquid. The term sorption is sometimes used to describe the take up of a gas or a liquid by a solid without explaining whether the process of take up is adsorption or absorption [10]. A pictorial comparison between adsorption and absorption is shown in figure 2.3.

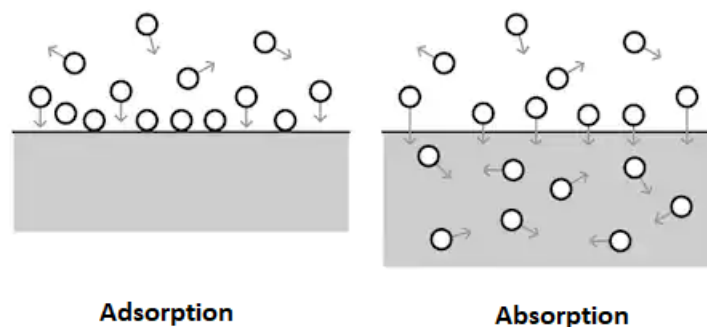


**Figure 2.3:** Difference between adsorption and absorption.

Further classification of adsorption process can be done based on whether the forces involved in adhesion are physical or chemical in nature. In physical adsorption, the force of attraction between the adsorbate molecule and adsorbent solid are the Van der Waal forces. These are weak dispersion forces that hold the adsorbate molecule onto the adsorbent. There is no chemical specificity involved in physical adsorption meaning any gas would adsorb onto any solid if the temperature is low enough and/or the pressure is high enough. In chemical adsorption, chemical bond formation occurs and hence this process is specific for each adsorbate and each adsorbent. In comparison to physical adsorption, chemical adsorption usually occurs at elevated

temperatures. Furthermore, the process is generally slower than physical adsorption and generally involves an activation energy.

## 2.2.2 Kinetics and equilibrium

To understand adsorption, it is important to know the adsorption equilibria information i.e. how much adsorbate can adsorb onto an adsorbent under certain conditions. A common characterization of adsorption equilibria is by the use of adsorption isotherms [11]. The isotherm relates the amount of adsorbate adsorbed onto an adsorbent to the partial pressure of the adsorbate in the gas phase. The temperature of the system is kept constant for each isotherm line.

Several models have been proposed over the years that describe the equilibrium isotherms for adsorption. Since the models are empirical or semi empirical, the models are restricted to certain pressure intervals and this should be kept in mind before implementing the models [12]. For this study, the Dubinin Astakhov isotherm is used to describe the adsorption equilibrium. This model was found to provide good results for n-butane adsorption onto activated carbon as stated by Möller [13].

### 2.2.2.1 Dubinin Astakhov Isotherm

The solids used as adsorbents in practical applications have complex structures and hence deviate from the basic fundamental description such as the Langmuir model [14]. The langmuir model explains the adsorption process using several assumptions which are not satisfied for real solids. Hence the basic langmuir isotherm equation does not describe the data well. This was also seen in the study conducted by Möller [13] who came to the conclusion that the Dubinin-Astakhov model provides better simulation results in comparison to Langmuir model. Dubinin-Astakhov model is a semi-empirical approach that is used to describe the equilibrium data.

This model is only applicable for microporous solids [14]. In this class of solids, micropore walls are in close proximity to each other, providing an enhanced adsorption potential within the micropores. This strong potential is due to the dispersive forces. Dubinin formulated his theory based on these forces and he termed the mechanism of adsorption as micropore filling. The Dubinin equation has its history in the development of theory for adsorption in activated carbon. Since the study in focus uses activated carbon, the Dubinin equation is used for simulations. Equation 2.1 shows the Dubinin Astakhov equation [14].

$$W = W_o \exp \left[ - \left( \frac{\epsilon}{E} \right)^n \right] \quad (2.1)$$

where  $W$  is mass of adsorbed species per unit volume of packed bed,  $W_o$  is the mass of adsorbed species per unit volume of packed bed at the saturation pressure, the parameter  $n$  describes the surface heterogeneity and  $\epsilon$  is the adsorption potential. With this parameter  $n$  in the adsorption isotherm equation, the Dubinin Astakhov equation provides flexibility in the description of adsorption data of many microporous solids ranging from a narrow to wide micropore size distribution.

The adsorption potential  $\epsilon$  is given by equation 2.2. It is described as the work required to compress the gas phase from pressure  $P$  to saturation pressure  $P_s$ :

$$\epsilon = \int_p^{p_s} \epsilon dp = RT \ln \left( \frac{p_s}{p} \right) \quad (2.2)$$

Substituting equation 2.1 in equation 2.2 we get equation 2.3,

$$\bar{\theta}^* = \frac{W}{W_o} = \exp \left[ - \left( \frac{RT \ln \left( \frac{p_s}{p} \right)}{E} \right)^n \right] \quad (2.3)$$

where  $\bar{\theta}^*$  is the equilibrium fractional coverage.

### 2.2.2.2 Isosteric heat of adsorption

Isosteric heat of adsorption is the change in enthalpy of adsorbate when it adsorbs onto an adsorbent. It gives the heat released per unit mass of adsorbed species at a fixed value of coverage of adsorbate onto the adsorbent. It acts as an indicator for the strength of the attractive forces acting between the adsorbate and the adsorbent. The reason for obtaining the heat of adsorption at a fixed coverage is because this heat of adsorption can change with variations in coverage. In a study conducted by Fiani et al. on granular activated carbon, it was found that the isosteric heat of adsorption resulting from adsorption of n-butane on the carbon was almost constant. The value was approximately 22.1 kJ/mol for loadings between 0 and 0.3 kg of n-butane per kg of carbon [15]. For simplification, a constant value of heat of adsorption was used while calibrating the 1D and 3D models.

### 2.2.3 Linear Driving Force (LDF) model

The Linear Driving Force (LDF) model is a concept that describes the rate at which an adsorbate (pure or in mixture with an inert component) adsorbs to an adsorbent particle [16]. This model is used frequently for modelling of adsorption columns due to its simplicity as well as physical and analytical consistency. In a previous study carried out by Möller [13], simulations with the LDF model were carried out using the Dubinin Astakhov isotherm as well as Langmuir isotherm. It was shown that the model employing Dubinin Astakhov isotherm was more accurate in comparison to Langmuir isotherm. Therefore for this study, the LDF model along with Dubinin Astakhov isotherm are used. The LDF equation is given by equation 2.4.

$$\frac{d\bar{c}(t)}{dt} = K_L [\bar{c}^*(t) - \bar{c}(t)] \quad (2.4)$$

where  $\bar{c}(t)$  denotes the average concentration of the adsorbate at time  $t$  in the adsorbent particle and  $\bar{c}^*(t)$  is the average concentration of adsorbate in the adsorbent particle at time  $t$  that would be observed if equilibrium was achieved between the solid phase and the fluid phase under prevailing conditions of temperature and pressure [16].  $k_L$  is the effective LDF mass transfer coefficient. Equation 2.1 shows that the gradient will be positive i.e. adsorbate will continue to adsorb onto the adsorbent

if the concentration of adsorbate on the adsorbent is lower than the equilibrium adsorption. On the other hand, if the concentration of adsorbate on adsorbent is higher than the equilibrium adsorption, than the gradient will be negative and the desorption process will occur. The adsorption can also be written in terms of coverage:

$$\frac{d\bar{\theta}(t)}{dt} = K_L [\bar{\theta}^*(t) - \bar{\theta}(t)] \quad (2.5)$$

One important assumption for this model is the zero temperature gradient across the radius of the adsorbent particle i.e. temperature anywhere on or inside the particles will be the same [16].

### 2.2.4 LDF model using Dubinin Astakhov isotherm

Substituing the equilibrium fraction coverage  $\bar{\theta}^*$  into the LDF model equation i.e. equation 2.5 in equation 2.2, we get the final form of the LDF model equation that is used in the simulations.

$$\frac{d\bar{\theta}(t)}{dt} = K_L \left[ \exp \left[ - \left( \frac{RT \ln \left( \frac{p_s}{p} \right)}{E} \right)^n \right] - \bar{\theta}(t) \right] \quad (2.6)$$

The value of the saturation pressure  $p_s$  was found using the Antoine equation which relates the saturation pressure of a species to the temperature of the system. The Antoine equation takes the form [17],

$$\log_{10}(p_s) = A - \frac{B}{C + T} \quad (2.7)$$

The pressure,  $p_s$ , is in bars while the temperature, T, is in Kelvin. In the above equation the constants A, B and C are component specific parameters valid for certain temperature ranges. For n-butane, there are two temperature ranges as provided by the National Institute of Standards and Technology (NIST) and are given in table 2.1 [18].

**Table 2.1:** Parameters for n-Butane used in the Antoine equation as given by NIST.

Temperature range (K)	A	B	C
195.11 - 272.81	3.85002	909.65	-36.146
272.66 - 425	4.35576	1175.581	-2.071

The values of E and n can be determined by fitting of n-butane experimental data to adsorption isotherm. Erik Östermark [19] fitted the experimental data provided by the activated carbon manufacturer, Ingevity, to fit the isotherm and determined the values of E, n and  $W_o$ . Since the experimental data for the isotherm was the same for this project as well, no isotherm fitting was done. Rather only the method of isotherm fitting was validated and found to be correct.

The values of  $E$ ,  $n$  and  $W_o$  used in this study were 18422 J/mol, 1.43 and 191.5 g/L respectively. Using these values, the result of the isotherm fitting is shown in figure 2.4. It can be seen that the isotherm fits very well at temperature of 25°C but it deviates from the experimental values at higher temperature of 100°C. This observation has some implications on the results obtained for purge gas heating experiments and are discussed in chapter 4.

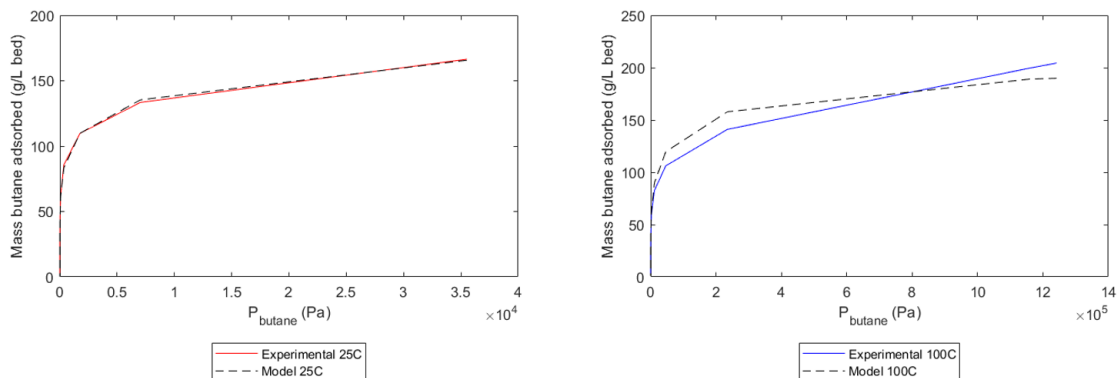


**Figure 2.4:** Isotherm fitting at temperature of 25° C (left) and 100° C (right) .

### 2.2.5 Activated carbon as adsorbent

The choice of adsorbent is a critical parameter that will effect the efficiency of the adsorption process [14]. A material that has good adsorption capacity but slower kinetics is not a good choice of adsorbent because slow kinetics imply that the adsorbate molecule would take a longer time to travel through the pore structure and reach the particle interior i.e. a greater mass transfer resistance is present [14]. In other word, this means that the gas residence time will be longer and the size of the porous bed would have to be larger to compensate for the longer residence time. On the other hand, if the kinetics are fast but the adsorption capacity of the material is low, more mass of adsorbent would be required for a given inflow of adsorbate [14]. A material that possesses both fast kinetics and higher loading capacity would be an ideal choice. To summarize, an adsorbent material should satisfy the following criteria:

- The solid material should possess high surface area or micropore volume,
- The porous network of the adsorbent should be relatively large to enable efficient transport of adsorbate molecules to the solid interior.

To fulfill the first requirement, the pore size of the porous material must be small and at the same time having good porosity. This means that a good porous solid should have both micropores as well as macropores. The classification of pore sizes as recommended by IUPAC (International Union of Pure and Applied Chemistry) is shown below [14]:

- Micropores  $d < 2$  nm,
- Mesopores  $2 < d < 50$  nm,

- Macropores  $d > 50$  nm.

The common porous materials used right now in industries include activated carbon, zeolites, alumina, silica gel etc. Among these solids, activated carbon have very wide range of application because of its high surface area and micropore volume. Activated carbon structure is made up of microcrystallites of graphite. These microcrystallites are arranged in a random orientation and the resulting spaces between the crystals form the micropore volume. The pore size distribution of activated carbon is typically trimodal meaning simultaneous presence of micropores, mesopores and macropores [14].

Typical ranges and properties of these three kinds of pores are given in table 2.2. These values are taken from the book 'Principles of Adsorption and Adsorption Processes' by D. M. Ruthven [14].

**Table 2.2:** Pore sizes and their properties in typical activated carbons.

	Micropores	Mesopores	Macropores
Diameter (nm)	$<2$	2 - 50	$>50$
Pore volume ( $\text{cm}^3/g$ )	0.15 - 0.5	0.02 - 0.1	0.2 - 0.5
Surface area ( $\text{m}^2/g$ )	100 - 1000	10 - 100	0.5 - 2

It can be seen in table 2.2 that the surface area of macropores is negligible in comparison to the micropore area and hence they are of little significance when it comes to adsorption capacity. Instead they are considered to be transport channels that allow transfer of adsorbate molecules from the bulk solid phase to the particle interior i.e. mesopores and micropores.

The intermediate pore size is termed mesopores. These pores have a greater surface area in comparison to the macropores. The mesopores contribute to the adsorption capacity to a varying extent, depending on the thermodynamic conditions. These pores also act as transport pores for the adsorbate molecules.

Micropores are spaces in between the microcrystallites that have sufficiently high adsorption/dispersive forces to adsorb the adsorbate molecule. The micropores provide the majority of the space for storage and the mechanism of adsorption is explained by the process of pore volume filling [14].

## 2.3 Computational Fluid Dynamics (CFD)

Nowadays, Computational Fluid Dynamics (CFD) is being used in a wide variety of applications such as automotive industry, shipping industry, turbomachinery etc. It primarily involves the numerical solution of the equation of motion to predict the flow behavior of a fluid. Coupled with additional models, CFD becomes a powerful tool to accurately predict more complex behaviours such as turbulence, multiphase flows, reactive flows etc. CFD offers a variety of advantages. A product design can be tested on computer software without ever building a prototype. Also, it enables

the user to modify design easily and test for the same conditions which would otherwise take a lot of time if experimental prototypes were physically build.

For this study, the flow across a cylindrical carbon canister was modelled using CFD tools. Since the adsorption process is highly dependent on the prevailing conditions inside the carbon bed such as temperature and pressure as well as n-butane concentration, it is important to predict the gas flow through the carbon bed since these thermodynamic properties and concentration will vary if the flow field inside the canister varies. Also, since the system is non-isothermal, heat transfer plays an important role and since heat transfer is dependent on fluid flow rates, the accuracy of the simulation models would be greatly influenced by the resolution of flow field.

In this section, the methods for modelling of flow physics are discussed. Even though in principle, the governing equations solved are the same for both 1D and 3D cases, their formulations differ. Also, since two different softwares are used for 1D and 3D simulations, the approaches used vary as well. Hence, the 1D and 3D modelling is discussed separately.

### 2.3.1 1D/2D modelling in GT Suite

In a 1D model, the governing equations for fluid flow are solved for one spatial coordinate and time. Before any governing equation can be solved, the system needs to be sub divided into control volumes called cells [20]. The collection of these cells form the grid. In what is known as the staggered grid approach, the cell is represented by its volume and its boundaries. The cell can interact with neighbouring cells and exchange mass, heat and momentum. The scalar quantities such as temperature or density are represented by a single value for the cell and these values are uniform anywhere inside the cell. The vector quantities, such as velocity and fluxes, are stored at the cell boundaries [20].

For resolving the fluid flow through the cells, the software solves the governing equations which are the conservation equations for mass, energy and momentum. Equation 2.8 is the equation for conservation of mass, also known as the continuity equation.

$$\frac{dm}{dt} = \sum_{boundaries} \dot{m} \quad (2.8)$$

where  $\dot{m} = \rho uA$ , where  $\rho$  is the density of the fluid, A is the cross sectional area through which the fluid is moving and u is the fluid velocity. The energy equation, in terms of specific enthalpy, is as given by equation 2.9.

$$\frac{d(\rho HV)}{dt} = \sum_{boundaries} (\dot{m}H) + V \frac{dp}{dt} - hA_s(T_{fluid} - T_{wall}) \quad (2.9)$$

where V is the volume of cell, H is the total specific enthalpy,  $A_s$  is the surface area available for heat transfer across the walls, h is the heat transfer coefficient,  $T_{fluid}$  is

the temperature of the fluid while  $T_{wall}$  is the wall temperature. The conservation equation for momentum is given by equation 2.10.

$$\frac{d(\dot{m})}{dt} = \frac{dpA + \sum_{boundaries}(\dot{m}u) - 4C_f \frac{\rho u |u|}{2} \frac{dxA}{D} - K_p(\frac{1}{2}\rho u |u|)A}{dx} \quad (2.10)$$

where  $dp$  is pressure differential acting across distance  $dx$ ,  $A$  is the cross sectional flow area,  $u$  is the velocity at the boundary,  $C_f$  is the fanning friction factor,  $D$  is the equivalent diameter and  $K_p$  is the pressure loss coefficient.

The above equations are applicable for flow through open channels such as pipes. Special treatment is required for modelling the flow through packed beds where the randomness of particles produces a random distribution of flow channels inbetween the particles. It is difficult to resolve the flow through these openings since the exact dimensions of these channels would be required and these very small openings would further be discretized into even smaller cells for solving the governing equations. Instead, empirical correlations are used which describe the mass, energy and momentum transfer across a packed bed [21].

As the fluid moves through the openings inside the packed bed, the drag force (friction force) results in a loss of momentum of the flowing fluid. As a result, a pressure drop is observed. For modelling the packed bed, it is essential that the pressure drop is accurately depicted since the pressure drop directly impacts the flow field inside the packed bed. Pressure drop across the bed is given by equation 2.11.

$$f = \frac{\varepsilon_b^3}{S_v(1 - \varepsilon_b)} \frac{\Delta P}{L} \frac{1}{\rho U_o^2} \quad (2.11)$$

where  $\Delta P$  is the pressure drop of the packed bed of length  $L$ ,  $U_o$  is the superficial velocity of fluid and  $f$  is the friction factor. The friction factor,  $f$ , is given by the Ergun equation. The Ergun equation formulation used in GT-SUITE is given by equation 2.12.

$$f = \left(\frac{1 - \varepsilon_b}{2\varepsilon_b^2}\right) \left(\frac{150}{Re_b} + 1.75\right) \quad (2.12)$$

where  $\varepsilon_b$  is the bed porosity and  $Re_b$  is the Reynolds number which is given by equation 2.13.

$$Re = \frac{D_p}{1 - \varepsilon_b} \frac{\rho \varepsilon_b \nu}{\mu} \quad (2.13)$$

where  $D_p$  is the effective particle diameter and the chosen characteristic length for packed bed.  $\rho$  is the fluid density,  $\nu$  is the fluid velocity and  $\mu$  is the fluid dynamic viscosity. The effective particle diameter is given by equation 2.14.

$$D_p = \frac{6(1 - \varepsilon_b)}{S} \quad (2.14)$$

where  $S$  is the specific surface area of particles.

Since there are two phases present inside the packed bed i.e. the solid phase (particles) and the gas phase, an energy equation will need to be solved for both phases. The solid phase energy equation is given by equation 2.15.

$$\Psi \frac{dT_s}{dt} = \frac{d}{dx} \left( F_s \lambda_s \frac{dT_s}{dx} \right) + hS(T_f - T_s) - \sum_k \Delta H_{R,k} \cdot r_k + \frac{P}{V} + h_{ex} S_{ex} (T_{ex} - T_s) \quad (2.15)$$

where  $\Psi$  is the effective heat capacity of the reactor,  $T_s$  is the temperature of solid phase,  $F_s$  is the solid fraction inside the bed,  $\lambda_s$  is the thermal conductivity of the particles,  $h$  is the heat transfer coefficient,  $S$  is the surface area per reactor volume,  $\Delta H_{R,k}$  is the enthalpy of reaction,  $r_k$  is the rate of reaction,  $P$  is the power input,  $V$  is the reactor volume,  $h_{ex}$  is the external heat transfer coefficient,  $S_{ex}$  is the external surface area per reactor volume and  $T_{ex}$  is the external temperature.

The gas phase energy equation is shown in equation 2.16.

$$\varepsilon_b \rho c_p \frac{dT_f}{dt} + \varepsilon_b \rho c_p u_{is} \frac{dT_f}{dx} = hS(T_s - T_f) \quad (2.16)$$

where  $c_p$  is the specific heat capacity of the fluid and  $h$  is the interphase heat transfer coefficient.

There is an option in GT-SUITE for modelling of heat transfer in 2D. This is achieved by application of fourier law of heat conduction across the radial discretization of the packed bed. The heat transfer from one volume to the next in radial direction is given by equation 2.17.

$$q_{radial} = \lambda_s \frac{\Delta T_{s,radial}}{\Delta R_{radial}} \quad (2.17)$$

where  $\Delta T_{s,radial}$  is the temperature difference between solids of two adjacent volumes in radial direction and  $\Delta R_{radial}$  is the discretization length in the radial direction. The continuity equation for the packed bed is given by equation 2.18.

$$\frac{d\rho}{dt} + \frac{d}{dx}(\rho u_{is}) = 0 \quad (2.18)$$

The momentum equation is given by equation 2.19.

$$\varepsilon_b \frac{dP}{dx} + \varepsilon_b \frac{d}{dt}(\rho u_{is}) + \varepsilon_b u_{is} \frac{d}{dx}(\rho u_{is}) = -Sf \frac{1}{2} \rho u_{is}^2 \quad (2.19)$$

where  $S$  is the surface area per reactor volume and  $f$  is the friction factor. Mass balance for gas phase species is given by equation 2.20.

$$\varepsilon_b \rho \frac{d}{dt}(\Omega_{f,j}) + \varepsilon_b \rho u_{is} \frac{d}{dx}(\Omega_{f,j}) = \sum_K \sigma_{j,k} \cdot r_k \quad (2.20)$$

where  $\Omega_{f,j}$  is the mass fraction of species  $j$  in the fluid phase and  $\sigma_{j,k}$  is the stoichiometric coefficient of species  $j$  in the reaction. In the case of adsorption, the assumption is that only one molecule of adsorbate binds with one active site hence

this coefficient is equal to 1.

There is a condition imposed on every cell which ensures that the sum of all coverages i.e. empty site coverage and adsorbed site coverage, must equal one. This is represented by equation 2.21.

$$\sum_{K_j} \Theta_j = 1 \quad (2.21)$$

### 2.3.2 3D Modelling in Star CCM+

Similar to 1D simulations, the mass, energy and momentum equations are solved in 3D simulations. The only difference is that in 3D simulations, these equations are solved across three different boundaries i.e. three directions ( $x_1, x_2, x_3$ ). Hence, the governing equations are also written in three dimensional forms. The continuity equation becomes [22]:

$$\frac{\partial \rho}{\partial t} + \frac{\partial \rho U_1}{\partial x_1} + \frac{\partial \rho U_2}{\partial x_2} + \frac{\partial \rho U_3}{\partial x_3} = 0 \quad (2.22)$$

Equation 2.22 can be written in tensor notation form. The equation is written as,

$$\frac{\partial \rho}{\partial t} + \frac{\partial \rho U_j}{\partial x_j} = 0 \quad (2.23)$$

In 3D case, j can be 1, 2 or 3 and represents the three directions. For the following equations, the tensor notation is applied for simplification.

It is difficult to solve the continuity equation numerically so in CFD program, a combination of continuity equation and momentum equation is used. The resulting equation is called the Poisson equation for pressure [23]. For constant viscosity and density the poisson equation is shown below:

$$\frac{\partial}{\partial x_i} \left( \frac{\partial P}{\partial x_i} \right) = - \frac{\partial}{\partial x_i} \left[ \frac{\partial (\partial U_i U_j)}{\partial x_j} \right] \quad (2.24)$$

The momentum equation, derived from newton's 2nd law of motion is given by [23],

$$\frac{\partial U_i}{\partial t} + \sum_j \frac{\partial U_i}{\partial x_j} = - \frac{1}{\rho} \frac{\partial P}{\partial x_i} + \sum_j \frac{1}{\rho} \frac{\partial \tau_{ji}}{\partial x_j} + g_i \quad (2.25)$$

The above formulation is what is known as the Navier Stokes equations. The Navier Stokes equations are used for simulation of velocity and pressure. The poisson equation, shown above, is used to solve for pressure as a dependent variable and velocity is found by solving the momentum equation [23].

The energy equation is formulated by implementing the first law of thermodynamics across a control volume boundaries. The governing equation for energy is shown below,

$$\frac{\partial(\rho c_p T)}{\partial t} = -U_j \frac{\partial(\rho c_p T)}{\partial x_j} + \lambda \frac{\partial^2 T}{\partial x_j \partial x_j} - P \frac{\partial U_j}{\partial x_j} + \tau_{ij} \frac{\partial U_i}{\partial x_j} + \sum_n R_n(C, T)(-\Delta H_n) + S_T \quad (2.26)$$

In the above equation, the terms from left to right indicate accumulation, convection, conduction, expansion, dissipation, reaction source term and general source term. For the 3D model, the heat of adsorption released and gained during loading and purging, respectively, is implemented as source term,  $S_T$ . The reaction term is not present.

The species source term is used to solve the transport of species across a control volume. For a constant density fluid, the species transport equation is,

$$\frac{\partial C_n}{\partial t} + U_j \frac{\partial C_n}{\partial x_j} = \frac{\partial}{\partial x_j} \left( D_n \frac{\partial C_n}{\partial x_j} \right) + R(C, T) + S_n \quad (2.27)$$

In the above equation, the terms from left to right indicate accumulation, convection, diffusion, the reaction source term and the general source term. In the 3D model, the mass adsorbed and desorbed during loading and purging, respectively, is implemented as a source term,  $S_n$ . The reaction term is not present.

The species source term,  $S_n$  is given by the following expression [24],

$$S_n = -(1 - \varepsilon_b) \rho_p M_{C_4H_{10}} \frac{\partial n}{\partial t} \quad (2.28)$$

where  $\rho_p$  is the pellet density of activated carbon ( $\text{kg}/\text{m}^3$ ),  $\varepsilon_b$  is the porosity of the carbon bed,  $M_{C_4H_{10}}$  is the molecular weight on n-Butane ( $\text{kg}/\text{mol}$ ),  $n$  is the dynamic adsorption ( $\text{mol}/\text{kg C}$ ) and  $t$  is the timestep.

In the species source term, the term  $\frac{\partial n}{\partial t}$  is the change in adsorption and is given by the LDF model. It should be noted that the equation 2.4 shows the LDF expression in terms of concentration. However, for ease of implementation and unit consistency in the 3D software, STAR-CCM+, the LDF model equation is written in terms of adsorption,  $n$ , with units of ( $\text{mol}/\text{kg C}$ ).

Similar to the LDF model, the Dubinin Astakhov equation is also written in terms of adsorption and is given by the following expression,

$$n^* = n_{max} \exp \left[ - \left( \frac{RT \ln \left( \frac{p_s}{p} \right)}{E} \right)^m \right] \quad (2.29)$$

Where  $n_{max}$  ( $\text{mol}/\text{kg Carbon}$ ) is the maximum adsorption and is the adsorption property of a specific adsorbate adsorbing onto an adsorbent.

The energy source term,  $S_T$  is given by the following expression [24],

$$S_T = - \frac{\Delta H S_n}{M_{C_4H_{10}}} \quad (2.30)$$

## 2. Theory

---

$\Delta H$  is the heat of adsorption (J/mol). This heat of adsorption is used as one of the tuning parameters in the calibration of 3D model.

# 3

## Experimental and simulation method

In this chapter, the methods employed for testing and evaluation of carbon canisters are discussed. These include both the experimental and the modelling approach. Some of the methods are built upon the previous work presented by Erik Östermark [19] and Erik Möller [13] while some additional methods have been introduced for better understanding of the inter-bed processes such as concentration profiles in the radial and axial directions.

### 3.1 Experiments

In order to validate the simulation results, its usually a good idea to verify them using experimental data. To achieve a good comparison, the operating conditions, boundary conditions and the geometry of the apparatus should be identical to the one used in the simulation. Furthermore, the adsorption model used in the simulation needs to be tuned to match the experimental results. The experiments provide the temperature and mass change data which is required for model calibration. The following sections elaborate on the approach used to obtain this data.

#### 3.1.1 Setup

In the previous study conducted by Erik Östermark [19], he studied the results of simulation for larger diameter canisters. He found that during loading and purging, the results for 1D and 2D simulations were identical for smaller diameters but started to deviate for larger diameter canisters. In order to investigate this further, this study was conducted on two carbon canisters of varying dimensions. Another motivation for constructing a larger sized canister was to obtain distinguishable gas samples in different radial positions which are difficult to obtain in a smaller sized canister.

##### 3.1.1.1 Large canister

The actual canister is shown in figure 3.1. This canister was filled with 5.38 litres (1560 grams) of BAX 1500 activated carbon from Ingevity.

### 3. Experimental and simulation method

---



**Figure 3.1:** The large experimental canister.

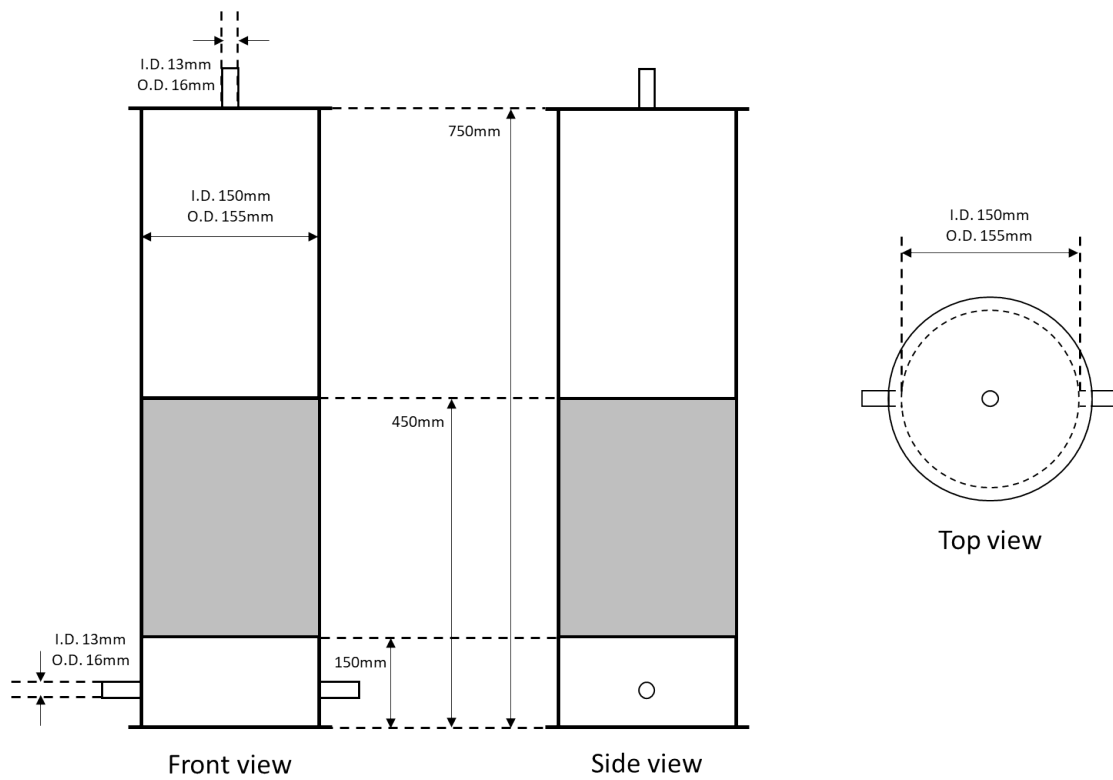


**Figure 3.2:** Large canister dimensions

**3.1.1.1.1 Canisters geometry** The canister dimensions are shown in figure 3.2. The body of the canister was made out of a PVC pipe. The carbon bed was compressed with the help of perforated plates and plastic foam on both the top and bottom sides and screwed in place. Connections were made on the top and bottom of the body using a smaller PVC pipe. The bottom connection couldn't be made at the very bottom because the canister was placed on a mass balance during experiments. Instead two connections at the bottom were made in the canister wall to maintain even distribution of the flow inside the canister.

**3.1.1.1.2 Sensors and sampling ports** The positions of thermocouples, gas syringe ports and pressure ports are shown in figure 3.3. In the large canister there are 17 thermocouples installed. There is one thermocouple each at the top and bottom of the canister which provides the inlet and outlet temperatures. There are 15 thermocouples inserted in the carbon bed. There are 5 thermocouples installed at each of the three axial positions (25%, 50% and 75% of the bed height). At each axial position the thermocouples are installed at different radial positions starting from wall to bed center.

There are 4 ports for pressure measurement. A port is located at both top and bottom of the perforated plate and plastic foam that are holding the bed at both the top and bottom of the carbon bed. The reason for having four ports is to measure pressure drop across the carbon bed both including and excluding the perforated plate and plastic foam.

There are 15 gas syringe needles inserted inside the carbon bed to collect gas samples. The positions of these syringes are similar to the thermocouple positions with slight variation in the radial positions.

**3.1.1.1.3 Insulation** The large canister was insulated with insulation foam at the location of the carbon bed after one set of loading and purging experiments were conducted without any insulation. The reason for insulating the canister was to see the extent of heat loss to the surrounding air during loading and heat gain from the surrounding air during purging. The small canister was not insulated.

#### 3.1.1.2 Small canister

The actual canister is shown in figure 3.4. This canister was filled with 0.5 litres (146.3 grams) of BAX 1500 activated carbon from Ingevity.

### 3. Experimental and simulation method

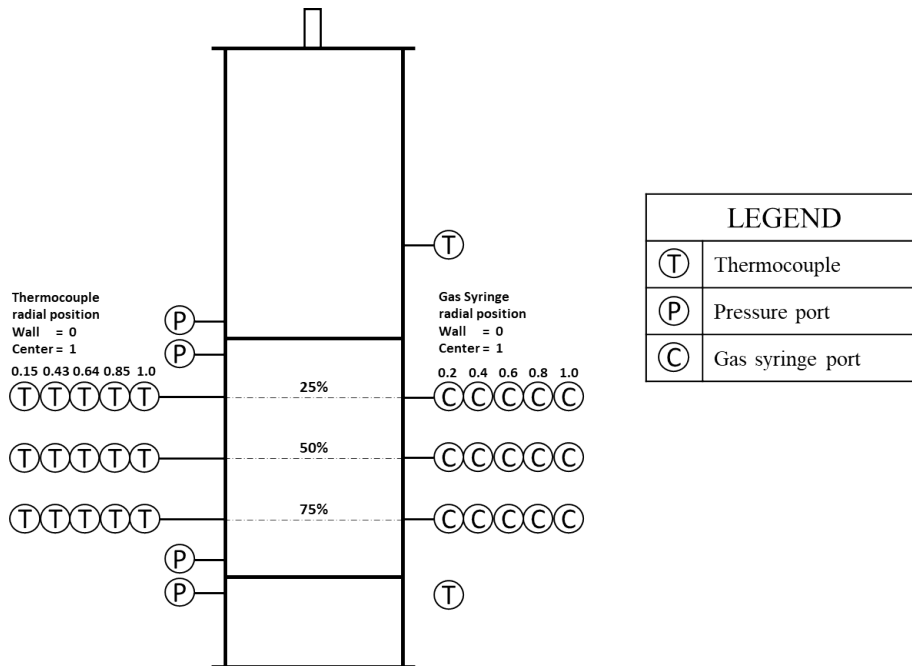


**Figure 3.3:** Large canister sensors and sampling ports positions



**Figure 3.4:** The small fabricated canister.

**3.1.1.2.1 Canisters geometry** The canister dimensions are shown in figure 3.5. Similar to the large canister, the body of the canister was made out of a PVC pipe and the carbon bed was compressed with the help of perforated plates and plastic foam on both top and bottom sides and screwed in place. Connection were

made on the top and bottom of the body using a smaller PVC pipe. The bottom connection could not be made at the very bottom because the canister was placed on a mass balance during experiments. Unlike the large canister, only one bottom connection was made for the smaller canister since the diameter of the pipe is small and having multiple connections will have little effect on flow distribution.

**3.1.1.2.2 Sensors and sampling ports** The positions of thermocouples, gas syringe ports and pressure ports are shown in figure 3.6. In the small canister there are 16 thermocouples installed. There are two thermocouple each at the top and bottom of the canister which provides the center and near wall temperatures at inlet and outlet of the open channel. There are 12 thermocouples inserted in the carbon bed. There are 3 thermocouples installed at each of the four axial positions (20%, 40%, 60% and 80% of the bed height). At each axial position the thermocouples are installed at different radial positions starting from wall to bed center.

The location of the pressure ports is similar to the large canister. There are 4 ports for pressure measurement. The reason for having four ports is to measure pressure drop across the carbon bed both including and excluding the perforated plate and plastic foam.

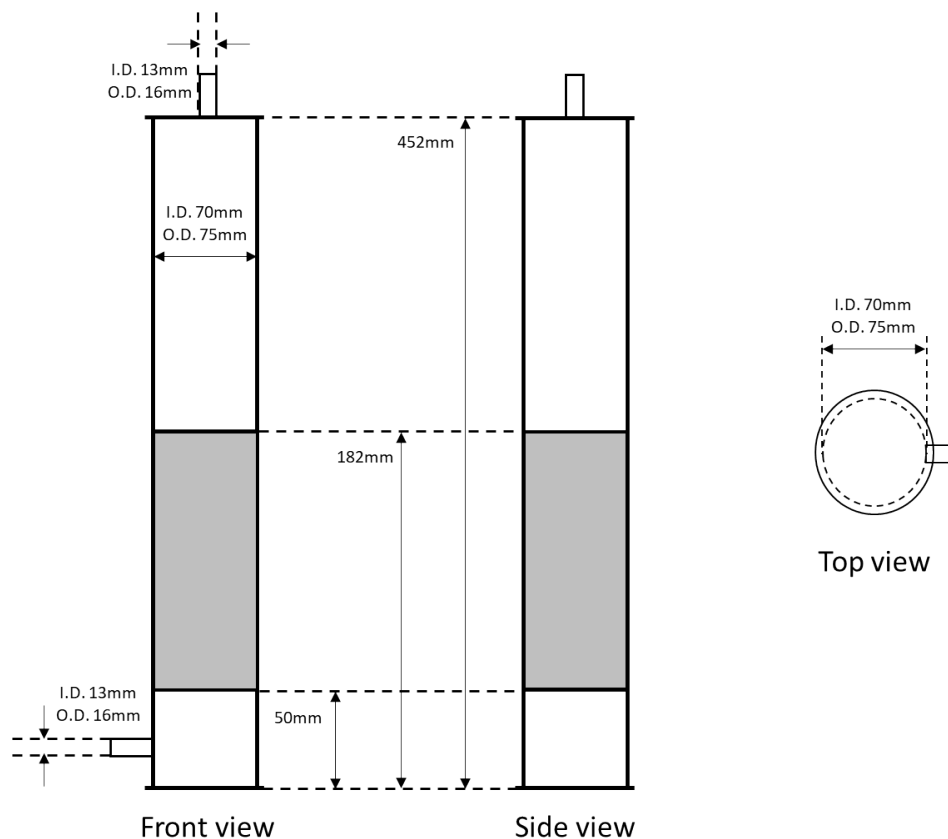


**Figure 3.5:** Small canister dimensions

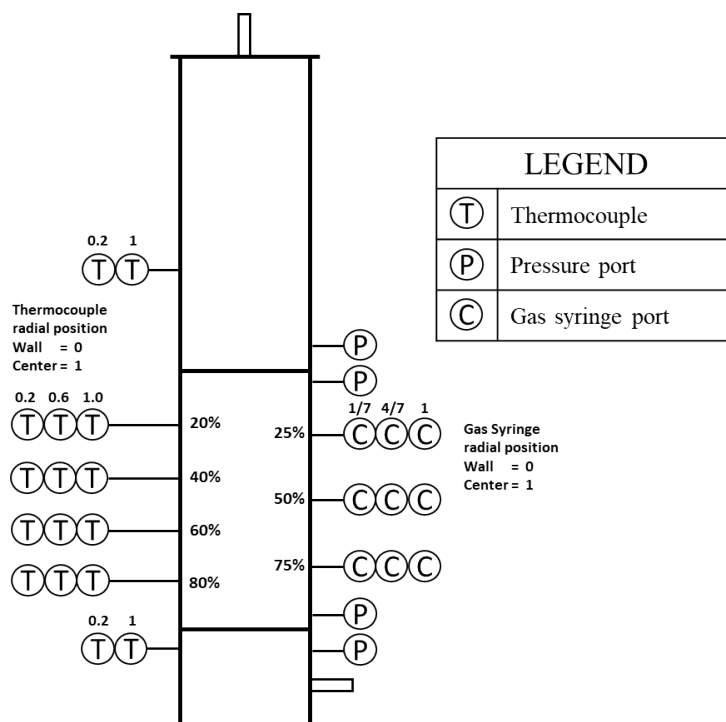


**Figure 3.6:** Small canister sensors and sampling ports positions

There are 9 gas syringe needles inserted inside the carbon bed to collect gas samples. The syringes are located at 3 axial positions (25%, 50% and 75% of the bed height). At each axial position, there are 3 syringes located at different radial positions from wall to bed center.

#### 3.1.1.3 Canister length to diameter (L/D) ratio

The pressure drop and cross sectional area are important parameters that need to be optimized to achieve an optimal canister design that minimizes pressure drop and maximizes the working capacity i.e. the amount of hydrocarbons held within the carbon bed. These parameters are optimized by selecting a good L/D ratio of the canister geometry. During purging, a larger L/D ratio leads to an increase in the localized airflow over the carbon bed resulting in a more effective removal of the adsorbed hydrocarbons. During purging, the flowrates are higher which results in less axial dispersion. On the other hand, too large a ratio would lead to excessive pressure drop across the bed. Generally a ratio of 2-3 is selected by canister manufacturers [5]. Therefore, the chosen L/D ratio for the larger and smaller canister was 2 and 1.89 respectively.

#### 3.1.1.4 Entrance length

For a non developed flow entering a conduit, there is a minimum distance that is required for the flow profile to fully develop. Ideally, for experimental purposes, the flow entering the porous bed should be fully developed. However, this would require a longer length of inlet channel. Due to the limitations regarding handling of the canister, this entrance length was disregarded. The pipe length above the

porous bed in smaller and larger canister were 270 mm and 300mm. Furthermore, it was concluded that the presence of foam and perforated plate at the carbon bed entrance would provide enough flow resistance so that the flow entering inside the carbon bed would be close to uniform i.e. no gradient in the radial direction.

### 3.1.1.5 Canister cycling

Before running any actual loading and purging experiments, both the canisters were cycled several times to age the canister. Cycling refers to the loading and purging of the canister. Since the carbon used was new, cycling would help achieve a minimum coverage of hydrocarbons inside the carbon bed. Cycling was stopped once the mass of the canister after each cycle was almost constant. The mass change during cycling of the small and large canister is shown in figure 3.7.

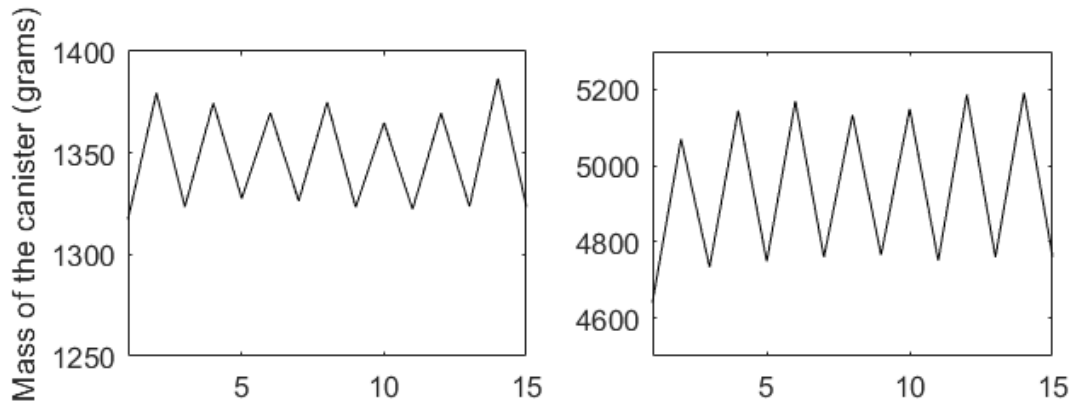


**Figure 3.7:** Mass change during cycling of small canister (left) and large canister (right).

## 3.1.2 Tests

This section will describe the procedure followed for carrying out the different kinds of experiments on both the large and small canister. The procedure followed for each canister is similar and any difference between the two procedures is mentioned in the following sections.

### 3.1.2.1 Pressure drop

Before running the simulation cases, it is vital to ensure that the flow characteristics in the model are the same as the one in the experiments. One way to achieve this is to validate that the pressure drop across the system, in this case the carbon bed, is the same for both the experiment and simulation. For this purpose, the pressure drop test was carried out on both the canisters.

Figure 3.8 shows the position of the pressure ports on the canister for pressure measurement during the pressure drop test. The test is carried out to obtain two pressure drop measurements i.e.  $\Delta P_{1-4}$  and  $\Delta P_{2-3}$ . The former is the pressure

### 3. Experimental and simulation method

---

drop across the entire carbon bed including the perforated plates and plastic foams while the latter excludes the perforated plates and plastic foam.

To run the test, the apparatus is connected to the test rig which supplies air flow to the canister from the top. The flow rate is gradually increased in increments and pressure drop is measured after each increment. The air flow rate and incremental increase in flow for both the canisters is shown in table 3.1.

**Table 3.1:** Experimental conditions for pressure drop test for both canisters.

	Small canister	Large canister
Air flow rate (lit/min)	0 - 100	0 - 200
Air flow increments (lit/min)	10	20

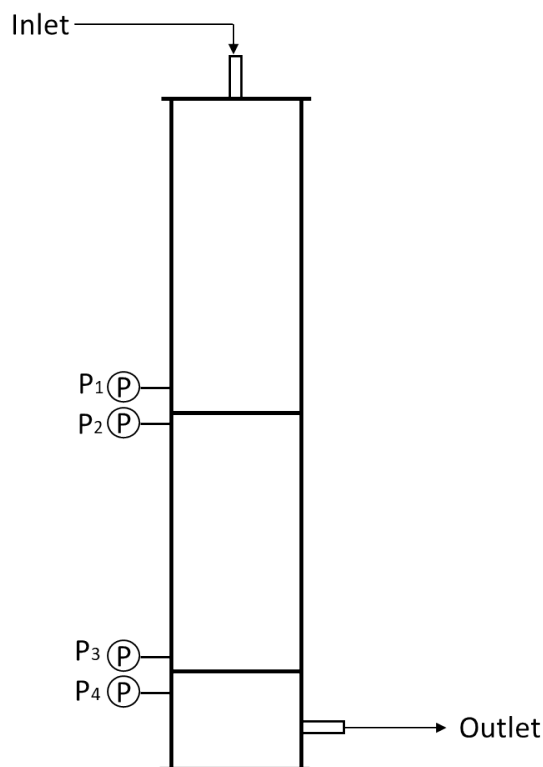


**Figure 3.8:** Position of pressure ports on the canister for pressure measurement.

#### 3.1.2.2 Loading

The pictorial view and the schematic for the loading experiment is shown in figure 3.9 and 3.10 respectively. During the loading experiment, the canister is placed on a mass balance and the mass reading was noted manually for the entire duration of the experiment. The loading experiment was carried out by flowing a mixture of 50%vol n-butane and 50%vol nitrogen from the canister top. The inlet flow was adjusted so that the butane flow was 40g/hr for the small canister and 60g/hr for the large canister. This was done by adjusting the rotameters that controlled the volumetric flow of Butane and nitrogen. The choice of 60g/hr butane flow rate for the large

canister was merely because of the fact that this was the maximum possible flow rate that was achievable with the available apparatus. Otherwise, a larger flow rate would have reduced the time for loading experiment of the large canister. The outlet of the canister was connected to another dummy canister. The dummy canister is also placed on a mass balance and it serves as an indicator for when the breakthrough of butane occurs from the actual canister. Once 2g of butane breakthrough is achieved, the loading experiment is stopped. The thermocouples are connected to a logging system and the temperatures at different regions inside the canister are monitored continuously. The gas samples are taken after 1.5 hrs of starting the experiment and then after every 30 minutes till the end of the experiment. Each collected sample is injected into the Automotive Emission Analyzer at one minute intervals. The analyzer signal is also continuously logged and the signals need to be processed afterwards to get actual butane concentrations.

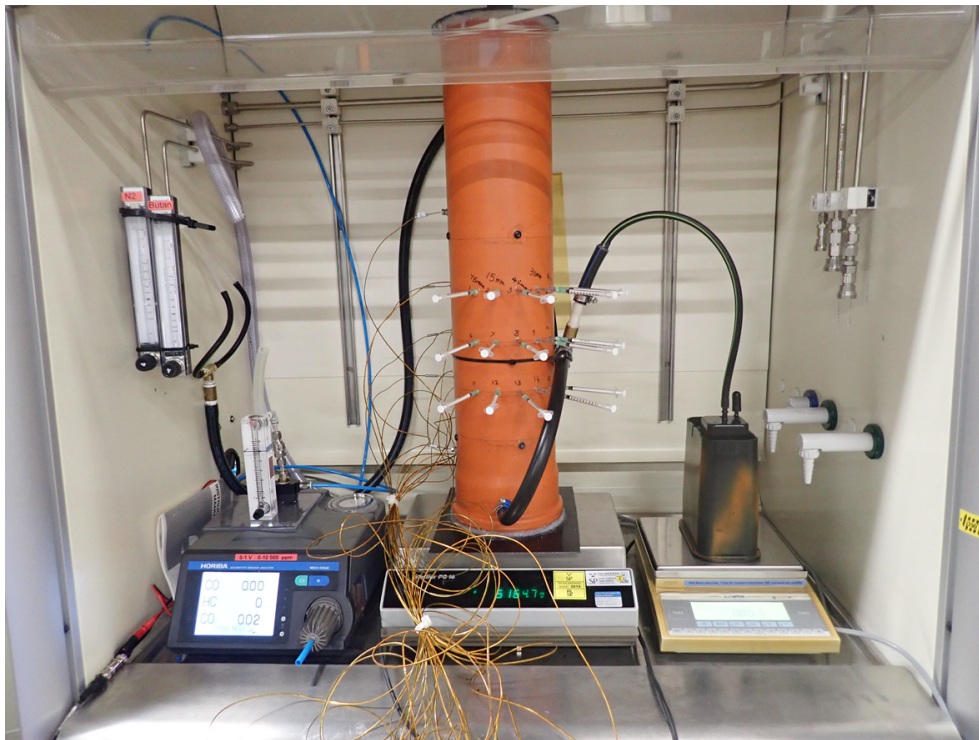


**Figure 3.9:** Experimental setup for loading of canister.

#### 3.1.2.3 Idle time

After each loading experiment was carried out, the canister was left to cool down to room temperature. This was referred to as 'idle time' during which the temperature inside the carbon bed was monitored. Once the temperature inside the carbon bed reached room temperature, the canister was ready for the purging experiment.

### 3. Experimental and simulation method

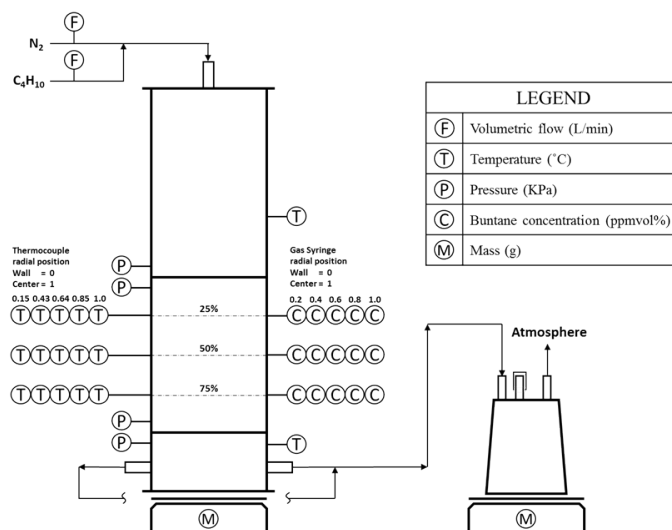


**Figure 3.10:** Schematic for the experimental setup during loading of canister.

#### 3.1.2.4 Purging

After the canister had reached room temperature after the loading experiment, the canister was ready for the purging experiment. The canister connections are removed and a new arrangement is done as shown in figure 3.11. The bottom ports of the canister are open to atmosphere while the top port is connected to an ejector via a rotameter. The ejector used high pressure air to create vacuum and hence a flow was established through the bottom of the canister and out the ejector. The ejector outlet was carefully placed inside the exhaust duct for safe removal of hydrocarbon vapors. Again, the canister was placed on a mass balance and the mass change was recorded manually until the end of the experiment. The purge flow rate was controlled by adjusting the rotameter. For the large canister, the purge flow was set to 30 lit/min while the flow rate for the small canister was set to 25 lit/min. Similar to the loading experiment, the temperatures and analyzer signals were monitored continuously throughout the experiment. The gas samples for the purging experiment were taken from the start and at smaller intervals of 10min and 15min for the small and large canister respectively. The purging experiment was stopped when the mass of the canister was nearly constant.

#### 3.1.2.5 Purge flow heating

As mentioned in the previous section, the purge flow experiments are conducted with atmospheric air at room temperature. To find the effect of heating the purge flow on the desorption process, a purge gas heater was used which heated the purge flow before it entered the canister. The purge flow heater was created by using a heating element of an air heater. The temperature of the air going out of the heater was controlled by varying the applied voltage across the heating element.

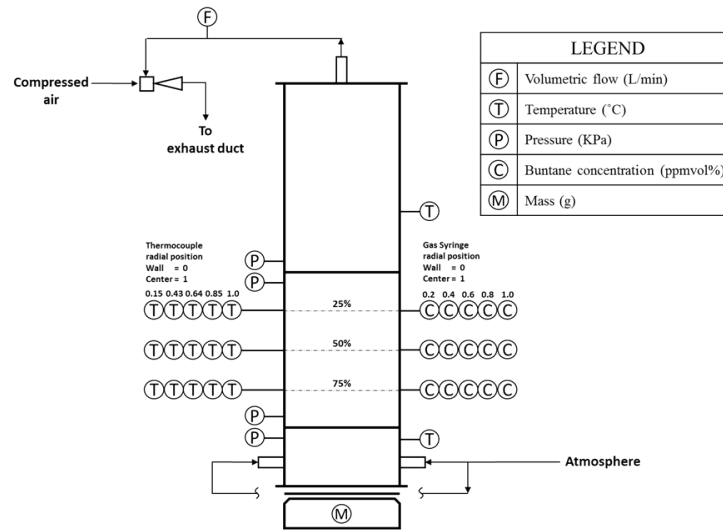


**Figure 3.11:** Experimental setup for purging of canister.

### 3.1.2.6 Gas sampling

The gas samples taken during the loading and purging experiments were analyzed by using the Automotive Emission Analyzer. The analyzer is meant for continuous detection but for the purpose of detecting gas samples the analyzer was run with its detection port open to atmosphere. The analyzer hydrocarbon signal was detected continuously. The gas sample was introduced into the inlet port of the analyzer and as a result a signal was obtained from the analyzer. In order to obtain the actual value of n-Butane in the gas sample, this signal was processed after the experiment.

The analyzer can detect Hydrocarbon levels in ppmvol and gives the Hexane equivalent value. To convert this value to n-Butane equivalent, the original value was multiplied by a factor,

$$Factor = \frac{Number\ of\ carbon\ atoms\ in\ Hexane}{Number\ of\ carbon\ atoms\ in\ Butane} = 1.5 \quad (3.1)$$

The signal or peak was integrated over the time the signal existed and the resulting value was multiplied by the Factor i.e. 1.5.

## 3.2 Simulations

Simulation of the carbon canister were performed in two programs, Gamma Technologies 'GT-SUITE' and Siemens PLM software 'STAR-CCM+'. 1D/2D simulations were performed in GT-SUITE while 3D simulations were carried out in STAR-CCM. 1D simulations were carried out for both the loading and purging cases while the 3D simulations were run for the loading case only. Furthermore, only the small canister was simulated using the 3D model and the large canister was out of scope because of the extremely high computational cost.

### 3.2.1 GT Suite

The 1D GT-SUITE model was created to simulate a single carbon bed with cylindrical geometry. The model is capable of simulating both the loading and purging processes. The simulation method and the model settings are largely based on the model developed by Erik Östermark [19]. However, the canister geometry is different and the model is modified to accommodate for these changes.

#### 3.2.1.1 Simulation Model

The GT-SUITE model schematic is shown in figure 3.12. There are different templates available in GT-SUITE that can be used to accurately depict the canister geometry as well as the adsorption model and the resulting mass transfer. In the underlying paragraphs, the functionality of each template is discussed.

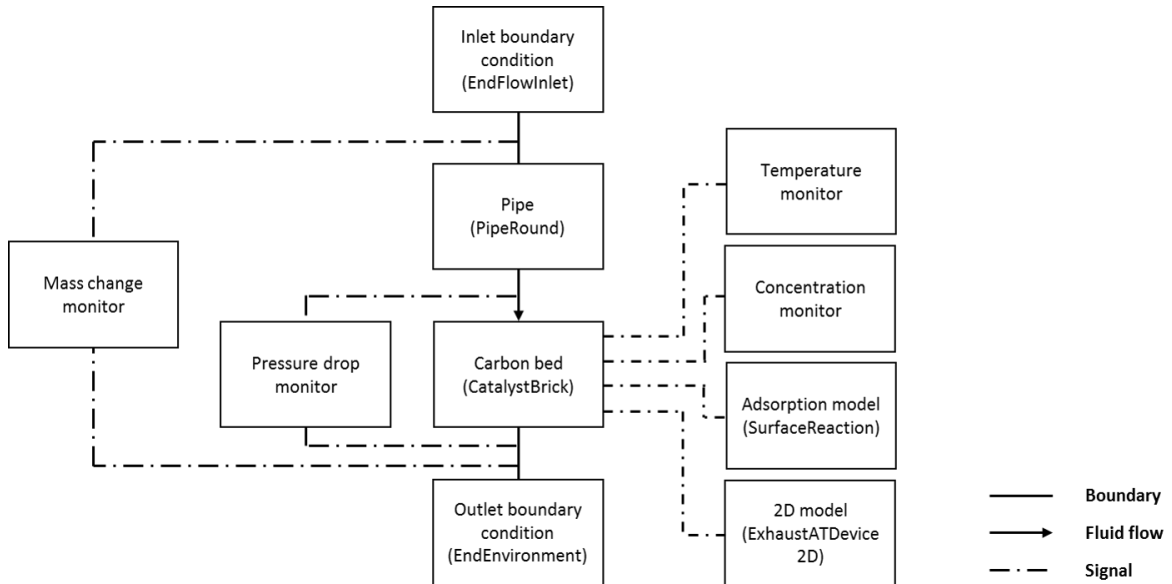


**Figure 3.12:** 1D model layout in GT-SUITE. The template titles in GT-SUITE are shown in brackets ().

To specify the system, the inlet and outlet boundary conditions needs to be set. There are several templates available for specifying different types of boundary conditions in GT-SUITE. For this simulation, the 'EndFlowInlet' template was used to specify the inlet condition. The inputs required by this template are:

- One of the following:
  - Volumetric flow rate,
  - Mass flow rate,
  - Velocity or
  - Mass flux.
- Temperature.
- Composition.

For this model, the inlet volumetric flow rate was specified along the temperature and composition. The boundary conditions used for the different cases are tabulated

in section 3.2.1.5.

The outlet boundary condition is specified by the template 'EndEnvironment'. The inputs for this template are:

- Absolute pressure,
- Temperature,
- Composition.

In addition to the above, additional conditions such as altitude and humidity can also be specified. The outlet boundary condition used for all the cases was the same except for the altitude variation cases where the altitude was specified as an additional parameter.

To include the open area above the carbon bed, as shown in figure 3.2 and 3.5, the 'PipeRound' template was used. This template models a pipe with round cross section. The following parameters were provided as inputs for this template:

- Pipe inlet and outlet diameter,
- Pipe length,
- Discretization length (length of individual sub-volumes),
- Wall material thermal properties and initial wall temperature.

Additionally, the thermal properties such as heat transfer correlations can be changed but for this study, these settings were set to default. The body force due to acceleration can also be specified and in this case, it was set to  $9.81 \text{ m/s}^2$  i.e. force due to gravity.

The 'CatalystBrick' template in GT-SUITE provides capabilities to model a flow through monolithic catalyst ('Standard channel geometry' selection in template) or a packed bed ('General geometry' selection in template). The parameters required by the template include:

- Frontal diameter/area,
- Bed length,
- Discretization length (length of individual sub-volumes),
- General geometry parameters (Specific area, solid fraction, f.Re and Nusselt number),
- Wall material thermal properties and initial wall temperature.

The template can be incorporated with a 2D model object to produce results in the radial direction as well. The specific area and solid fraction are physical properties of the BAX-1500 activated carbon and these values were taken from the model used by Erik Östermark [19] who obtained the BAX-1500 activated carbon data from the manufacturer, Ingevity [+].

The template 'SurfaceReactions' is used to incorporate the adsorption/desorption process and the mass transfer of butane that occurs during the process from the fluid phase to the solid phase. This template specifically deals with heterogeneous reaction mechanism. It calculates the coverage of the active site species and the

### 3. Experimental and simulation method

---

concentration expressions can be made functions of site coverage fractions. The inputs for this template included:

- Basis for the reaction rate (e.g. area, reactor volume or active site),
- Solver settings,
- Specification of site element(s), ,
- Coverage data (e.g. coverage species, initial coverage of species, enthalpy of formation of coverage species),
- Parameters for formulation of rate of reaction (e.g. pre-exponential multiplier, concentration expression).

For this study, the active site density was used as the basis for the rate expression with concentration specification in  $\text{mol}/\text{m}^3$ . This value was obtained from the BAX-1500 isotherm fitting results that was carried out by Erik Östermark [19]. This template also has an option for solving the diffusion inside the porous bed which would indicate whether the reaction is kinetics controlled or dependent on the mass transfer diffusion rate. If the diffusion is turned 'on', it means that the reaction rate is assumed to be equal to the mass transfer diffusion rate. If it is turned 'off', the reaction is kinetics limited and there is no gradient between the bulk phase and the surface concentration of the fluid phase. For this study, this option was turned 'off' and the effects of interphase mass transfer were incorporated into the pre-exponential factor,  $K_L$ , of the LDF model. It was noted by Erik Östermark [19] that there was a very small difference in results when the diffusion was turned 'on' so the effect of diffusion 'off' on the pre-exponential factor is likely to be small.

The 'ExhaustATDevice2D' template can be used to add 2D resolution of the carbon bed. This template is used along with the 'CatalystBrick' template. The number of radial zones needs to be defined and the radial heat transfer is solved for by implementation of equation [21] which solves for thermal conduction in the radial direction.

Several 'SignalMonitors' were also setup in the GT-SUITE model to log the simulation results. The monitors included:

- Pressure drop monitor across the porous bed (CatalystBrick),
- Mass change monitor for the porous bed,
- Temperature monitor for different positions inside the porous bed,
- Concentration monitor for different positions inside the porous bed.

The positions for temperature and concentration measurements inside the bed were selected to match the experimental measurement positions as shown in figure 3.3 and 3.6 for the large and small canister respectively.

The initial conditions for the model are shown in table 3.2.

**Table 3.2:** Initial conditions for the 1D GT-SUITE model for the loading and purging cases.

	Loading	Purging
Pressure (atm)	1	1
Temperature (C)	23	23
Composition (-)	50% Butane - 50% N2 mixture	Air

### 3.2.1.2 Numerical setup

In the 1D/2D GT-SUITE model, the implicit flow solver was used. In this method, all the equations are solved for all the sub-volumes simultaneously. This is achieved by iterative solution of a non-linear system of algebraic equations. The advantage of using the implicit method is that a relatively large time step can be made resulting in faster computational speed. The larger time step outweighs the increased computational cost of performing iterations for every time step. It is stated in GT-SUITE template help that this method should only be used if the wave dynamics are not important and the maximum mach number of the system is less than 0.3. All the cases solved for in this study satisfy these criteria so implicit solver was used for every case. The time step for the implicit solver is a user defined input in GT-SUITE. The time step used in the 1D/2D model was 0.02s and the number of iterations per time step were set to 1000.

Discretization is the division of a part resulting in sub-volumes. In CFD, the fundamental equations, such a continuity, energy and momentum equations, are solved for these sub-volumes. This suggests that the computational time of the simulation would be in a direct relation with the number of sub-volumes in the system. The discretization length is a measure of the size of the sub-volume. If larger discretization lengths are used, the total number of sub-volumes would be lower which would result in lower computational time but this might result in lower accuracy. On the other hand, if this distance is lower, a more accurate solution can be obtained but with longer computational times. It should be noted that there is a limit at which further decrease in discretization length will no longer change the solution accuracy and any further decrease in discretization length would only result in an increased computational cost with no improvement in results. A good solution would be one that operates near this limit which would result in maximum possible accuracy and a reasonable computational time. Figure 3.13 shows the discretization in 1D and 2D. It can be seen that moving from 1D to 2D, the number of sub-volumes greatly increases.

In the 1D model, the discretization length (dx) for the carbon bed was 5mm while the inlet pipe discretization length was 25mm. For the 2D case, the carbon bed was split into 9 radial zones and the resulting discretization length (dy) was 3.89mm.

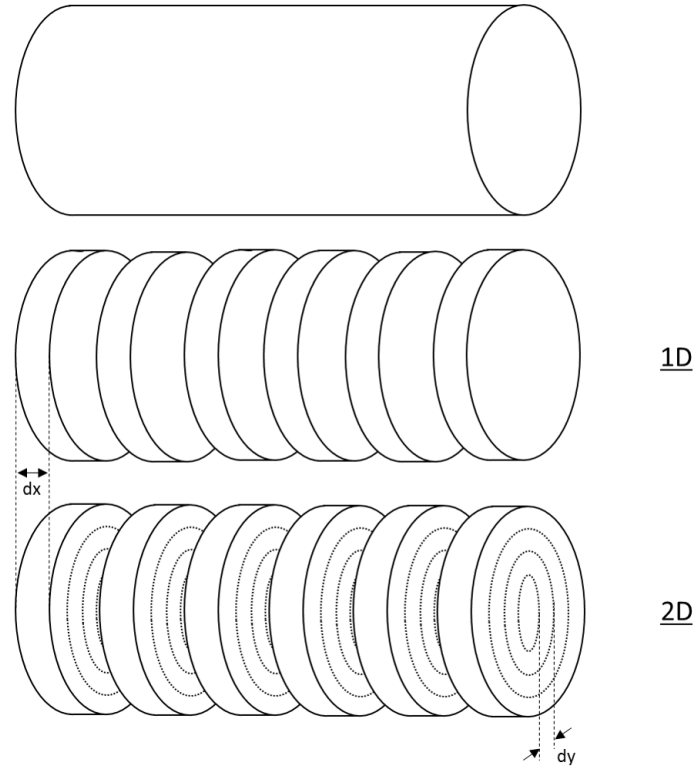


**Figure 3.13:** Discretization length representation for carbon bed in 1D and 2D.

### 3.2.1.3 Implementation of adsorption model

As mentioned in previous section, the template 'SurfaceReactions' is used to incorporate the adsorption model with the porous bed template 'CatalystBrick'. For an actual reaction, the expression for rate of reaction in GT-SUITE is given by,

$$R = A.T^b.exp(-T_a/T). \{conc\}.G(i).\theta(i) \quad (3.2)$$

where R is the reaction rate, A is the pre-exponential multiplier, T is the temperature, b is the temperature exponent,  $T_a$  is the activation temperature, conc is the concentration expression, G(i) is the general and inhibition functions and  $\theta(i)$  is the coverage expression.

For the adsorption case, equation 3.2 is simplified so the rate of reaction in terms of rate of change of coverage is given by the LDF model and is given by equation 3.3.

$$R = A \{conc\} \quad (3.3)$$

where  $A = K_L$ , which is the pre-exponential factor in the LDF model as given by equations 2.4-2.6. The concentration expression, in terms of equilibrium and dynamic coverage is given by,

$$\{conc\} = \theta^* - \theta \quad (3.4)$$

$\theta^*$  is the equilibrium coverage and is given by the Dubinin Astakhov isotherm.  $\theta$  is the dynamic coverage. The initial value of  $\theta$  for the empty and filled sites is an

input required by the software. The software then calculates  $\theta$  after each timestep by addition of the rate of change of coverage, obtained from equation 3.3, to the value of  $\theta$  before timestep.

#### 3.2.1.4 Calibration

Previous work regarding calibration of 1D model was performed by Erik Möller [13] and Erik Östermark [19]. This calibration was performed in GT-SUITE using the 'TotalErrorFunction' component. This component finds the difference between a signal and a set of measured data that the user specifies by varying the user specified tuning parameters. For the 1D model calibration, the experimental data provided was the change in mass of the canister and the carbon bed inlet and outlet temperatures. The set tuning parameters were the pre-exponential factor,  $K_L$ , and the heat of adsorption  $\Delta H$ . In the previous studies, it was concluded that for a carbon canister, the mass change of the canister was of primary concern and hence more weight was given to the mass change. In GT-SUITE, this was achieved by specifying the 'Weighting factor' inside 'TotalErrorFunction'. The value was set to 9 and 1 for mass change and temperature values respectively.

The model was run using the previous values of tuning parameters obtained by Erik Östermark [19] and it was found that the 1D model was showing very good agreement with experimental data of canister mass change. Hence, for all the simulation cases, the values of tuning parameters were kept the same as the previous study. The values of tuning parameters used are shown in table 3.3.

**Table 3.3:** Tuning parameter values for 1D GT-SUITE model.

Pre-exponential factor (-)	0.0025
Heat of Adsorption (kJ/mol)	-155

#### 3.2.1.5 Simulation cases

The simulation cases run on the 1D model are discussed in the following sections. The 1D model was used for simulation of both large and small canister. The 1D model was also used to do sensitivity analysis for purge gas heating and altitude change. The 2D model was used to simulate the small canister only since the computational time for solving the large canister was very large.

**3.2.1.5.1 Pressure drop** In the 1D model, the pressure drop across the carbon bed was validated with the experimental results. As mentioned before, in the experiments air flow was established across the carbon bed and pressure drop was measured at different flowrates of air. The same inlet condition was provided in the 1D model as shown in table 3.1. The pressure drop obtained from the model was then compared with the experimental results. The following cases were run:

1. Pressure drop across small canister for air flowrates between 0-100 L/min with 10 L/min increments.

### 3. Experimental and simulation method

---

2. Pressure drop across large canister for air flowrates between 0-200 L/min with 20 L/min increments.

**3.2.1.5.2 Loading** After the pressure drop results were matched and the tuning parameters were set, the model was run for loading and purging cases. For the canister loading the following cases were run in 1D model:

1. Small canister with inlet flowrate of 0.4 L/min of 50% Butane -50% Nitrogen mixture.
2. Large canister with inlet flowrate of 0.8 L/min of 50% Butane -50% Nitrogen mixture.

The following case(s) were run in 2D model:

1. Small canister with inlet flowrate of 0.8 L/min of 50% Butane -50% Nitrogen mixture.

**3.2.1.5.3 Purging** For the purging process the following cases were modelled in 1D model:

1. Small canister with inlet air flowrate of 25 L/min.
2. Large canister with inlet air flowrate of 30 L/min.

The following case(s) were run in 2D model:

1. Small canister with inlet air flowrate of 25 L/min.

**3.2.1.5.4 Purge gas heating** For testing the results of the purge gas heating, the 1D model was used. Instead of using a constant inlet air temperature, a transient time dependent temperature profile of inlet air, obtained from purge gas heating experiments, was used as input in the 1D model. The results of mass change of the canister were obtained for each case and compared with the experimental results. The inlet temperatures for different cases are shown in figure 3.14.

**3.2.1.5.5 Altitude** To see the effect of altitude variation on the canister performance during loading, 1D model was used and altitude at the outlet was varied. The following cases were run:

1. Sea level.
2. Altitude 1000m.
3. Altitude 2000m.
4. Altitude 3000m.

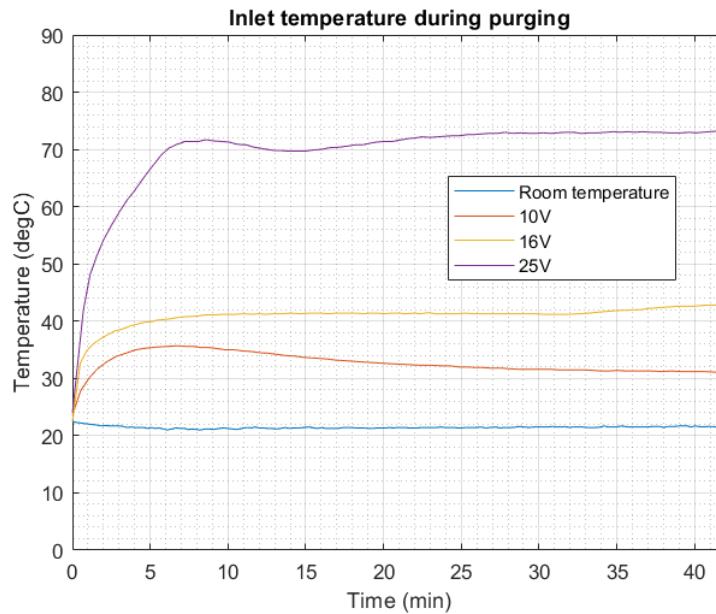


**Figure 3.14:** Inlet temperatures during purge gas heating experiments.

### 3.2.2 Star CCM+

The software STAR-CCM+ was used for 3D modelling of the canister. Since the processes to be simulated were quite long in real time, only the small canister was modelled. Furthermore, only the loading process was simulated with a higher flowrate of 0.8 L/min of 50% Butane -50% Nitrogen mixture.

#### 3.2.2.1 Geometry construction

The geometry for the small canister was constructed using the software, ANSA pre processor by BETA CAE solutions. The dimensions for the canister geometry were the same as those of the small experimental canister. the geometry is shown in figure 3.15.

The surface mesh for the geometry was also created in this software which was later imported into STAR-CCM+.

#### 3.2.2.2 3D model setup

Before running the simulations STAR-CCM+, the user has to provide some necessary inputs such as model selection, solver settings etc. The work flow required in STAR-CCM+ is shown in figure 3.16. A brief detail is also provided below.

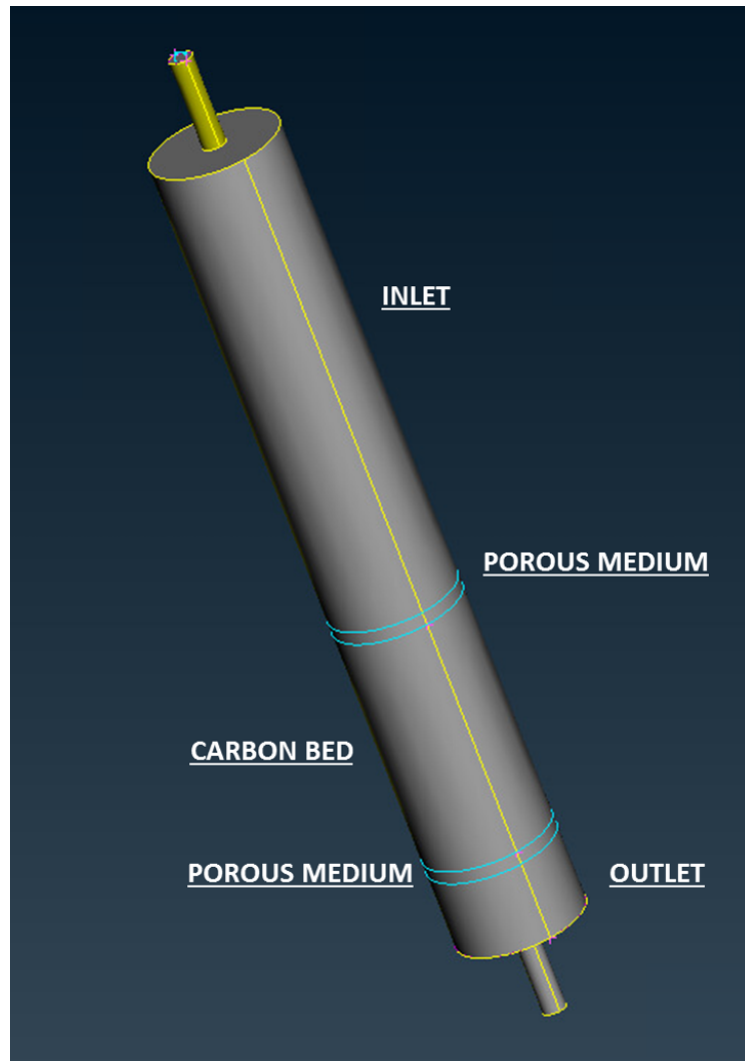


**Figure 3.15:** Small canister geometry as made in ANSA pre processor.

For setting up the 3D model, the surface mesh needs to be imported to the software. The surface mesh generated in ANSA pre processor is imported into the software. The geometry is split into different parts as per the surface topology. For the canister model, the geometry was split into five parts,

1. Inlet open channel.
2. Porous medium at inlet side.
3. Carbon bed.
4. Porous medium at outlet side.
5. Outlet open channel.

After splitting, these parts are assigned to regions and each region surface is assigned a boundary.

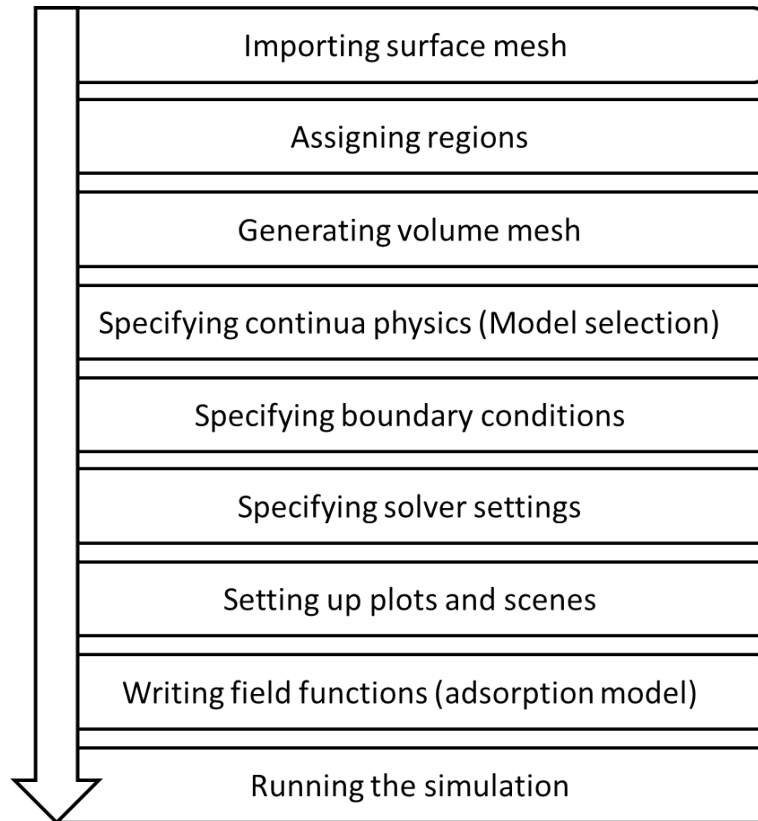


**Figure 3.16:** Small canister geometry as made in ANSA pre processor.

After specifying the regions, the volume mesh can be generated. For generating a mesh some inputs are required such as the type of mesh, cell size etc. The 'trimmed mesh' type was selected and the cell size was set to 1 mm.

To solve the 3D simulation, physics models need to be specified which provide the governing equations that the software ultimately solves. For the canister model, the following model selection was done.

- 3D model.
- Implicit unsteady.
- Laminar.
- Ideal gas.
- Constant density.
- Porous media model.
- Porous media drag model.
- Porous media thermal equilibrium.
- Multi-component gas.

Since the loading process is transient, the implicit unsteady model was selected. The flow characteristic was chosen to be laminar. This was done because the flow characteristic inside the carbon bed is laminar and since flow velocities are very small, the flow characteristic inside open channels could be characterised as laminar. This assumption was made to simplify the case and to speed up the simulation since moving to turbulence models means additional equations need to be solved which

increases computational cost.

The gases were assumed to follow the ideal gas law and the system was solved as a constant density system. The multi-component gas model was used to select the two gases present in the system i.e. n-Butane and Nitrogen.

To specify the carbon bed, the porous media model was chosen. The regions Porous medium at inlet side, carbon bed and Porous medium at outlet side were selected for this model. In this model the bed porosity and tortuosity can be input. The porous media drag model was used to calculate the pressure drop through the carbon bed. The porous media thermal equilibrium model was selected which establishes zero temperature gradient between the carbon bed solid particles and the gas phase.

The boundary conditions need to be specified for all the surfaces in the different regions. For the inlet region, the inlet boundary condition of 'mass flow inlet' was specified for the inlet surface. All the other surfaces for this region were specified as adiabatic wall boundary. For the porous medium at carbon bed inlet and outlet, the boundaries were specified as adiabatic walls. For the carbon bed, the heat loss to the surrounding was important so the wall boundary was set to convective heat transfer and convective heat transfer coefficient was specified. For the outlet region, the outlet surface was specified as 'pressure outlet' and all other surfaces were set to adiabatic wall boundary.

**3.2.2.2.1 Pressure drop** To obtain a pressure drop in the porous media, the porous media drag model was used. This model requires input of inertial and viscous resistances. These values were calibrated to obtain the same pressure drop as in the experimental case. For the calibration, a steady state simulation for the same geometry was run without any adsorption model equations using single component gas i.e. air. A constant isotropic tensor was used for the viscous resistance while the inertial resistance was ignored. The inertial tensor is only important if the Reynold's number is large but this was not the case.

The timestep for the implicit solver was chosen to be 50 ms and the solution time was near 40 min. Furthermore, plots were setup which continuously monitored the temperature and n-Butane concentration inside the carbon bed at the same locations as the thermocouples and gas syringes inside the experimental canister respectively. Additionally, scenes were setup to view the temperature variation and n-Butane concentration in the canister by setting up a 'derived part' which was a 2D symmetric plane cut of the canister.

**3.2.2.2.2 Adsorption model** In the 3D simulations, the adsorption model was setup using mass and energy source terms and writing equations in field functions. The species source term for n-Butane is given by equation 2.28 and the energy source term is given by equation 2.30. These equations are written with the help of field functions.

**3.2.2.2.3 Calibration** Similar to 1D model, the 3D model needs to be calibrated as well to match the experimental results. The tuning parameters were the pre-exponential factor,  $K_L$ , in LDF equation and heat of adsorption  $\Delta H$ . Unlike the 1D model in GT-SUITE where the optimization was carried out by the software using 'TotalErrorFunction', the calibration was performed in STAR-CCM+ manually. The values of tuning parameters were changed and the simulation result was compared with the experimental data. This was a time consuming process since the entire simulation had to be run for the results of a single set of tuning parameter values. The value of tuning parameter used for the final simulation are given in table 3.4.

**Table 3.4:** Tuning parameter values for 3D STAR-CCM+ model.

Pre-exponential factor (-)	0.0035
Heat of Adsorption (kJ/mol)	-18



# 4

## Results and discussion

In this chapter, the results and findings of the experiments and simulations will be discussed. The flow profiles and behaviours observed during experiments are stated and the underlying causes for these behaviours are explained. The results of the simulation models, both 1D and 3D, are shown and a comparison is made between experimental results and simulation results. The differences between the results are mentioned and reasoning is provided for these differences. In the plots shown in this chapter, the following nomenclature is used:

1. The plots for temperature and concentration profiles are shown at different axial positions inside the bed and shown in terms of percentage of the bed. The 0% position refers to the top of the bed and 100% position refers to the bottom of the bed.
2. In the plots showing results for different radial positions, the radial distance is shown as distance in mm from wall. This means that 0 mm refers to wall position and all the other values are distances from wall towards bed center.

### 4.1 Pressure drop

For modelling purposes, it is crucial that the pressure drop across the porous bed be known. The pressure drop directly affects the flow profile and since the adsorption model equations are strongly coupled with the flow behaviour, the pressure drop needs to be matched perfectly with the actual experimental results and validated. The pressure drop measured across the experimental canisters are shown in figure 4.1.

In the plots, the higher pressure drop line includes the pressure drop associated with the foam and perforated plates used both on top and bottom of the bed. The low pressure drop line only measures pressure drop across the activated carbon bed.

The pressure drop obtained using the 1D and 3D model are shown in figure 4.2. It can be seen that the 1D model made in GT-SUITE almost overlaps the experimental pressure drop line for large canister while it over estimates the pressure drop for the small canister. This deviation is associated with the fact that the pressure ports for the small canister were not located perfectly near the carbon bed top and bottom and the pressure difference reading was excluding some length of the bed resulting in a lower pressure drop in experimental results.

## 4. Results and discussion

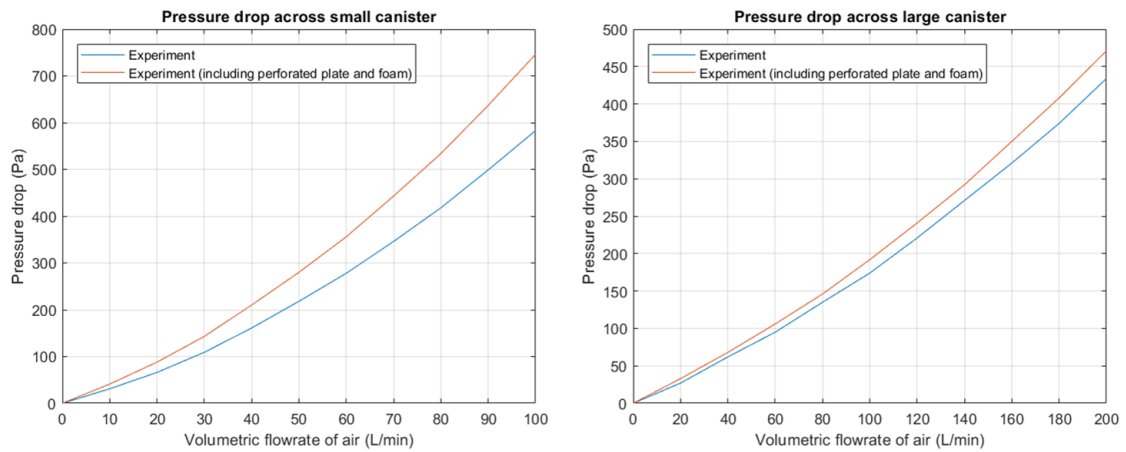


**Figure 4.1:** Pressure drop across the small canister (left) and large canister (right).

For the 3D model made in STAR-CCM+, constant user specified resistances for porous drag model were provided which resulted in a linear increase in pressure drop with increase in flowrate. It can be seen that at low flowrates, the model over estimates the pressure drop while it underestimates the pressure drop at higher flowrates. A pressure drop plot quite close to the experimental results was achieved by implementing the ergun equation as field function in STAR-CCM+ but at very low flowrates, the model was having instabilities. Since, the 3D model was used to simulate the loading case in which case the flowrate is less than 1 L/min, the simulation was simplified by use of user defined resistances which are close enough to experimental results at very low flowrates.

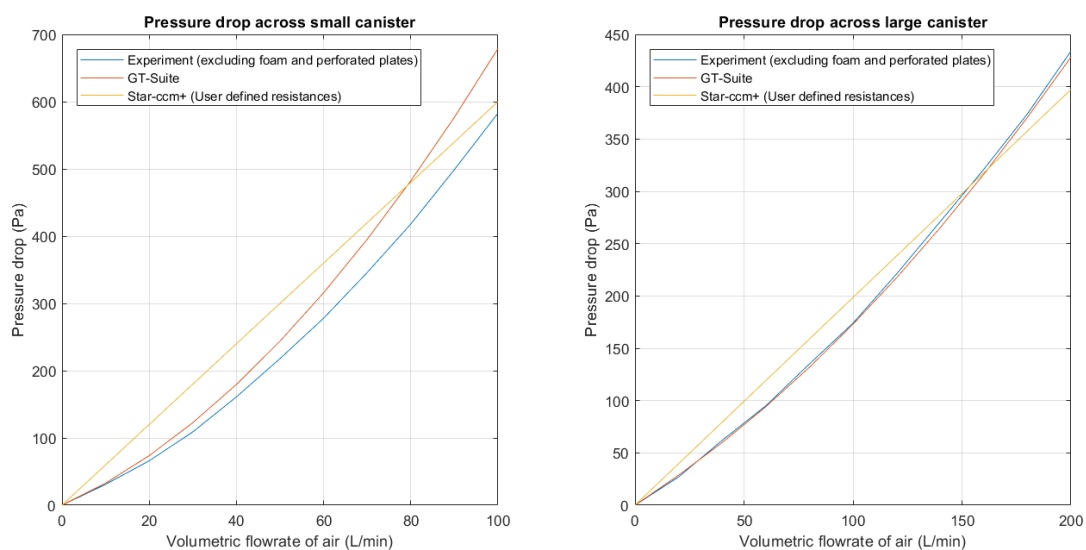


**Figure 4.2:** Comparison of pressure drop obtained by experiment and simulation across the carbon bed in small canister (left) and large canister (right) .

## 4.2 Loading

As stated before, for loading experiments, the following loading experiments were carried out,

1. Small canister loading with inlet flowrate of 0.4 L/min of 50% Butane and 50% nitrogen mixture by volume.
2. Small canister loading with inlet flowrate of 0.8 L/min of 50% Butane and 50% nitrogen mixture by volume.
3. Large uninsulated canister with inlet flowrate of 0.8 L/min of 50% Butane and 50% nitrogen mixture by volume.
4. Large insulated canister with inlet flowrate of 0.8 L/min of 50% Butane and 50% nitrogen mixture by volume.

Since the profiles are very similar, only the experimental results of one case for each canister are shown here. These are experiment (1) and (3) as shown above. The comparison between insulated and uninsulated canister is discussed in a separate section.

### 4.2.1 Small canister

Figures 4.3 and 4.4 show the mass change and temperature profiles, respectively, for the small canister loading experiments. For a normal loading case, the small canister mass gain was between 40-45g before breakthrough was achieved. The mass change was more or less linear and the deviations were caused by the fact that the canister was connected to pipes and a large number of wires and very slight movement resulted in mass scale reading variation.

Due to the exothermic adsorption process, the temperature inside the carbon bed increases. This temperature rise is highest in the bed center and lower near the wall. This radial temperature gradient is caused by heat loss to the atmosphere from the canister walls. As the butane becomes adsorbed onto the carbon, the temperature rises. The heat released is distributed in three forms:

1. Heat loss to the surrounding via the walls,
2. Heat transferred downstream via the incoming flow of nitrogen and
3. Heat retained by the activated carbon pellets.

After the carbon becomes saturated, the temperature rise stops and instead the incoming flowrate starts to cool the carbon. This can be seen in figure 4.4 where first the temperature increase is observed and after a maximum value is achieved the temperature starts to go down.

From the isotherm data of BAX1500, provided by Ingevity, the equilibrium adsorption is reduced by 45% when the temperature is increased from 100°F to 180°F. As can be seen in the temperature plots, there is a difference of about 40°C between the bed center and near wall temperatures. This means that the equilibrium adsorption of the activated carbon in the radial direction will also vary with lower values in bed center and higher values near the wall.

## 4. Results and discussion

---

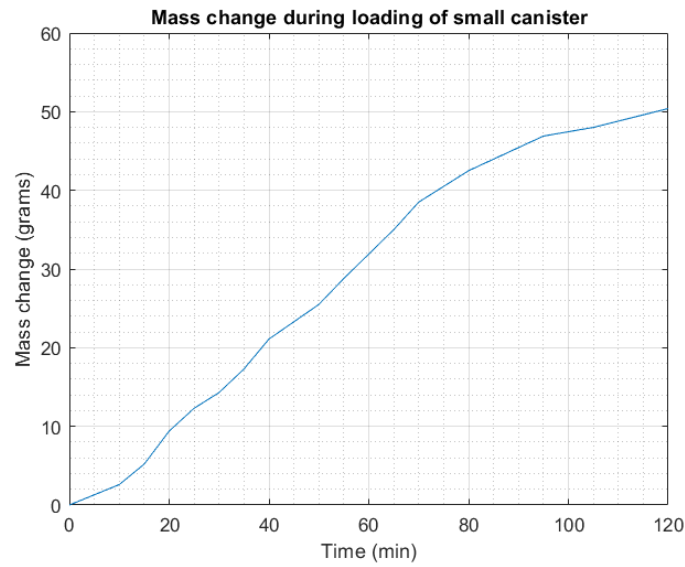


**Figure 4.3:** Mass change during loading of small canister.

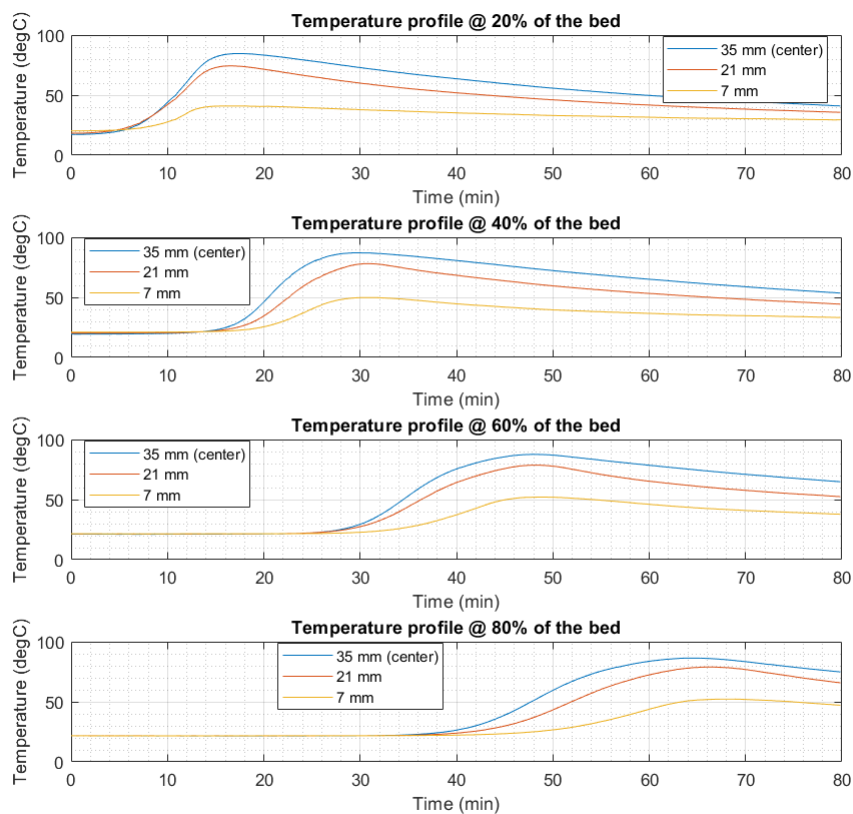


**Figure 4.4:** Temperature change during loading of small canister at four axial positions. For each axial position, the temperature at three radial positions are plotted.

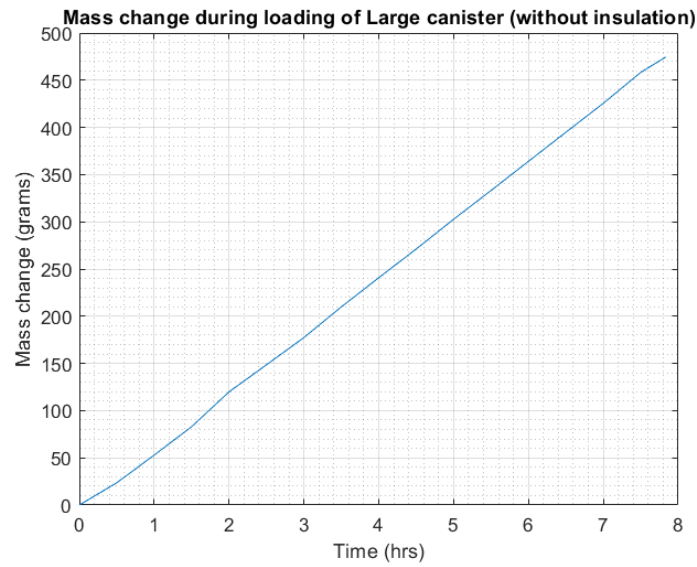


**Figure 4.5:** Mass change during loading of large canister (without insulation).

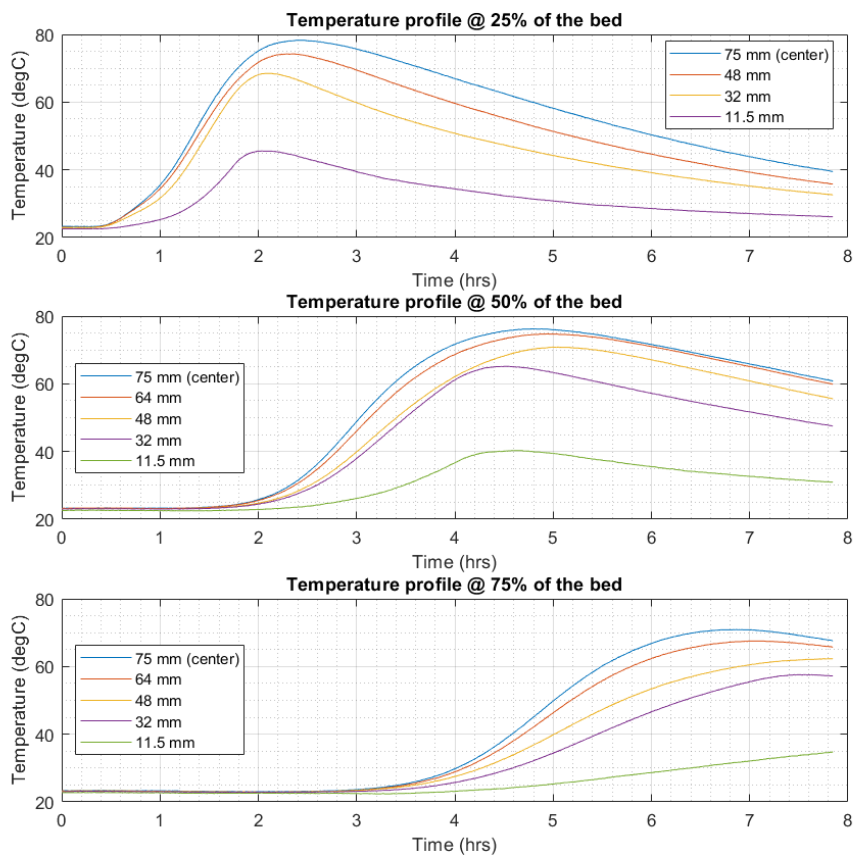


**Figure 4.6:** Temperature change during loading of large canister (without insulation) at three axial positions. The radial positions are shown as distance from the wall in each plot.

This also means that the adsorption potential i.e. the rate of adsorption will be different along different radial positions since the gradient of adsorption will be different. This gradient is the difference between the equilibrium adsorption and the dynamic adsorption at any given time.

### 4.2.2 Large canister (Without insulation)

Figures 4.5 and 4.6 show the mass change and temperature profiles, respectively, for the large uninsulated canister loading experiments. The mass gain for the large canister was about 450-480g before breakthrough occurs. As compared to the small canister, the large canister has about ten times more activated carbon and the time taken before breakthrough occurs is roughly ten times more for the same inlet flowrate of butane. The temperature profiles achieved are similar to the ones achieved for the small canister.

## 4.3 Purging

For the purging process, the following experiments were carried out:

1. Small canister purging with inlet flowrate of 25 L/min of air.
2. Large canister purging with inlet flowrate of 30 L/min of air.
3. Small canister purging with inlet flowrate of 25 L/min of air at higher temperature using purge gas heater.

Cases 1 and 2 are discussed in this section and the case with purge gas heating is discussed in a separate section.

### 4.3.1 Small canister

Figure 4.7 and 4.8 show the mass change and temperature profiles, respectively, for the small canister purging experiments. For a flowrate of 25 L/min of air at room temperature, a mass loss of approximately 50g is observed. At the start of purging, the rate of change in mass is very high and as time goes on the mass loss of canister slows down and ultimately reaches an almost constant value. Since desorption is an endothermic process, a temperature drop is observed inside the carbon bed. This temperature drop is quite steep in the first few minutes and can be associated with the higher mass loss that occurs initially. This low temperature zone causes the following heat transfer processes,

1. Heat transfer from the surrounding into the carbon bed near the bed wall,
2. Heat transfer from the relatively hot air inflow to the carbon bed pellets.

When the rate of heat required for desorption becomes less than the rate of heat gained from the above mentioned heat transfer processes the temperature in the bed starts to rise.

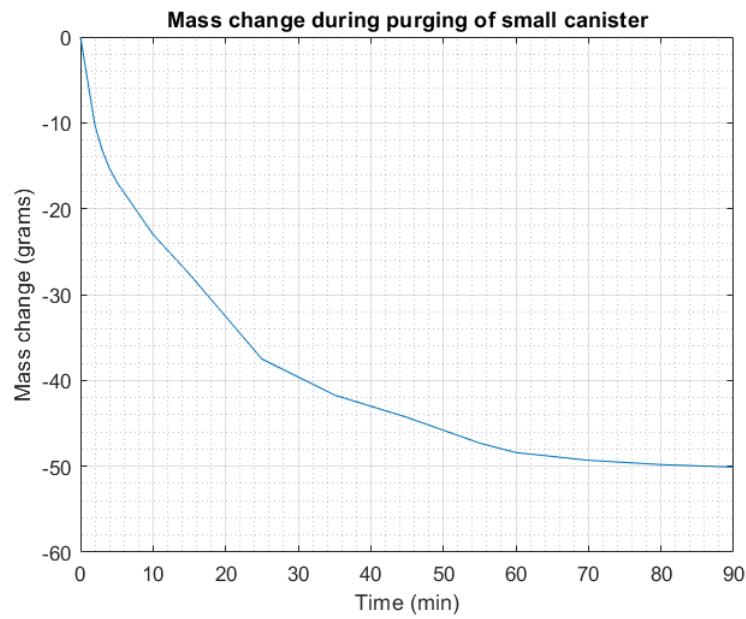


Figure 4.7: Mass change during purging of small canister.

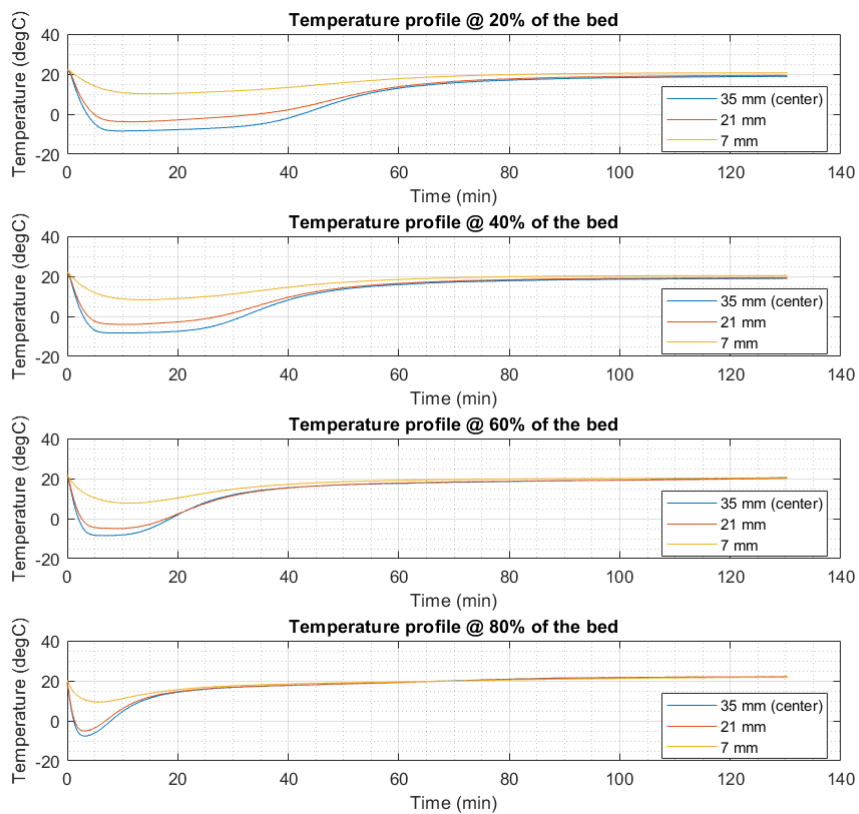
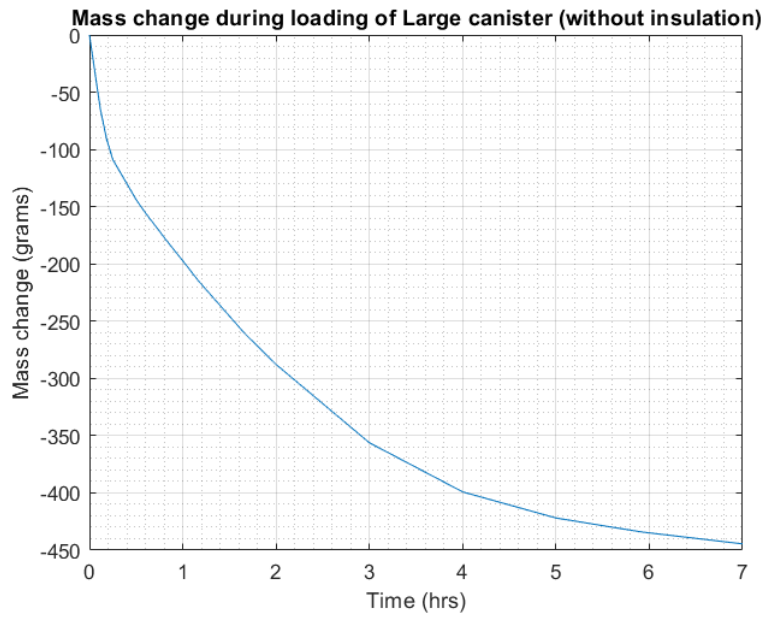
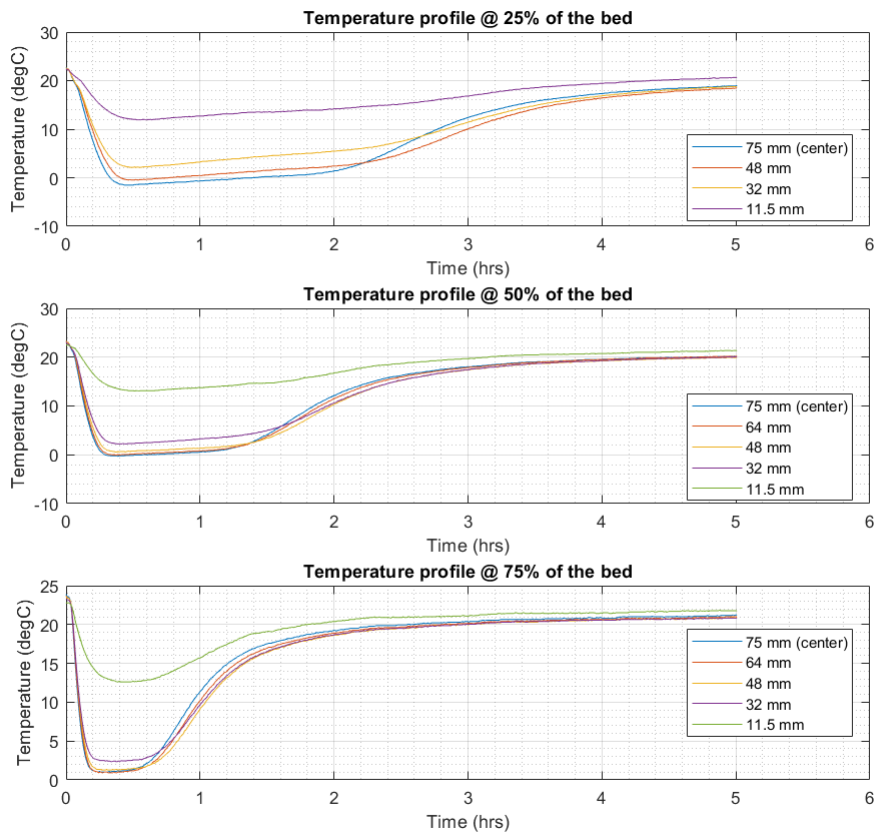


Figure 4.8: Temperature change during purging of small canister at four axial positions.



**Figure 4.9:** Mass change during purging of large canister (without insulation).



**Figure 4.10:** Temperature change during purging of large canister (without insulation) at three axial positions.

### 4.3.2 Large canister (Without insulation)

Figure 4.9 and 4.10 show the mass change and temperature profiles, respectively, for the large uninsulated canister purging experiments. The mass loss for the large canister is about 450g. Similar to the small canister, a sharp mass change is observed initially and the rate of change in mass drops as time goes on until it reaches an almost zero value. The temperature profiles are similar to the ones obtained for small canister. The volumetric flux in this canister is lower than that for smaller canister. This is because of the fact that a maximum purge flowrate of 30 L/min was achieved with the available experimental apparatus. This was a limitation since the larger canister would have a lower flux in comparison to the smaller canister and so the flow conditions inside the carbon bed of the two canisters would be different.

## 4.4 Simulation results

This section will discuss the results obtained from the 1D and 3D models. A comparison between the simulation results and experimental results is also shown and the differences and causes of deviations are discussed.

As explained earlier in chapter 3, the majority of the cases run in simulations were for small canister only. The exception being the 1D modelling of large canister. This was done to reduce the computational cost of these simulations.

### 4.4.1 Butane Storage (Loading)

As mentioned earlier, the mass change of a canister, especially during loading, is of primary interest since this provides information such as canister storage capacity and breakthrough time which are crucial parameters when testing for bleed emissions from the canister. Hence, while calibrating the models, both 1D and 3D, the primary target result was to match the mass change.

Figure 4.11 shows the 1D model results for the loading and purging processes as compared to the experimental results. For the loading process, the initial empty site coverage fraction was set to 0.76. This meant that 24% of the active sites were filled at the start of loading. This value was an approximate guess value obtained from the initial cycling data as discussed in section 3.1.1.5. For the purging process, the initial empty site coverage was set to 0.2. There was no possible way to know this value experimentally so the value which best fit the experimental result was chosen for this purpose.

It can be seen that the mass change obtained by the 1D model has very good agreement with the experimental results. However, as will be shown later, the temperature profiles are greatly overestimated.

Figure 4.12 shows the results of the 3D model along with the 1D model and experimental results. It can be seen that the 3D simulation results deviate from the

## 4. Results and discussion

experimental ones and two observations can be made. Firstly, the 3D model has a low mass gain in first few minutes and secondly, the breakthrough is achieved earlier than the experimental results. This to be expected since the 3D model was not fully calibrated.

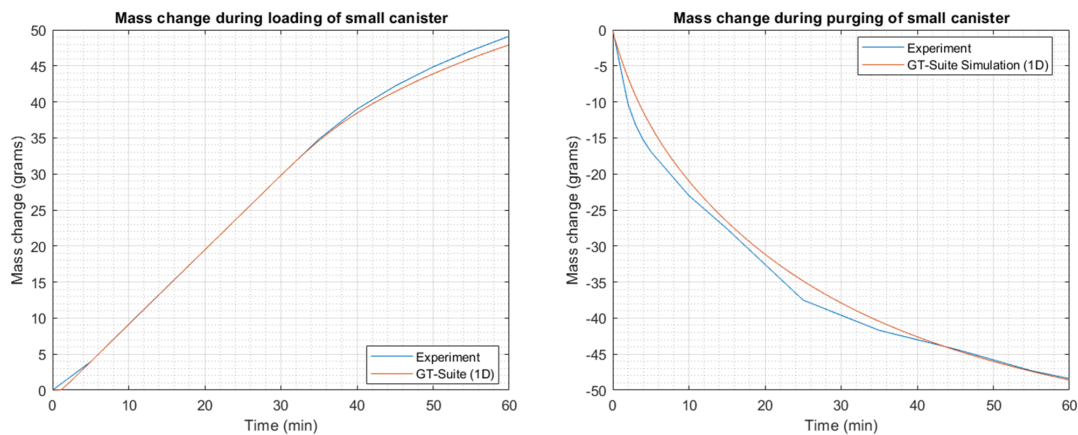


**Figure 4.11:** Mass change during loading (left) and purging (right) for experiment and 1D simulation.

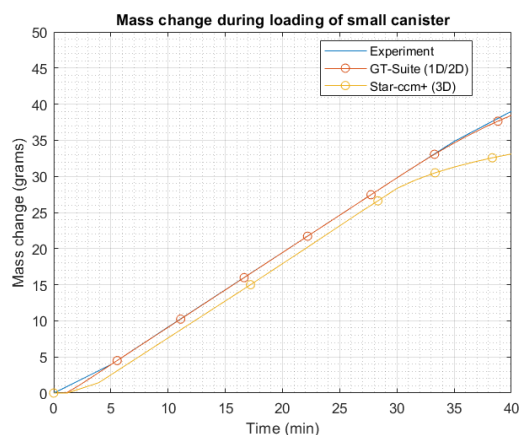


**Figure 4.12:** Comparison of mass change during loading between experimental and simulation results.

Unlike the 1D model where the software was able to tune the tuning parameters, in the 3D model this was done manually. Furthermore, in addition to the calibration of tuning parameters  $K_L$  and  $\Delta H$ , the values of maximum adsorption,  $n_{max}$ , and dynamic adsorption,  $n$ , were also unknown. The value of  $n_{max}$  is a property of a particular adsorbate adsorbing onto an adsorbent. Unfortunately, this value was not known. Furthermore, the dynamic adsorption,  $n$ , initial value was also guessed. It should be noted that  $n/n_{max}$  gives the coverage of the filled active site. For the final simulation, the values used for calibration are given in table 4.1.

The value of dynamic adsorption shown in table 4.1 corresponds to an initial filled active site coverage of 0.3. This is a quite high value and limits the adsorption

capacity of the bed in the 3D model. Due to lack of time, no further calibration was done. With a lower coverage, the loading capacity would be higher and a better fit can be expected with the experimental results. It can also fix the issue of earlier breakthrough that is seen in figure 4.12.

**Table 4.1:** Calibration parameters for 3D model.

Pre-exponential factor, $K_L$ (-)	0.0035
Heat of Adsorption, $\Delta H$ (kJ/mol)	-18
Maximum adsorption, $n_{max}$ (mol/kg C)	8.249
Dynamic Adsorption, $n$ (mol/kg C)	2.475

#### 4.4.2 Temperature profiles

Figure 4.13 shows the temperature profiles obtained by the 1D and 3D models along with the experimental results. It can be seen that both models overestimate the temperature profiles. However, the temperature profiles for the 3D model are closer to the experimental values than the 1D model.

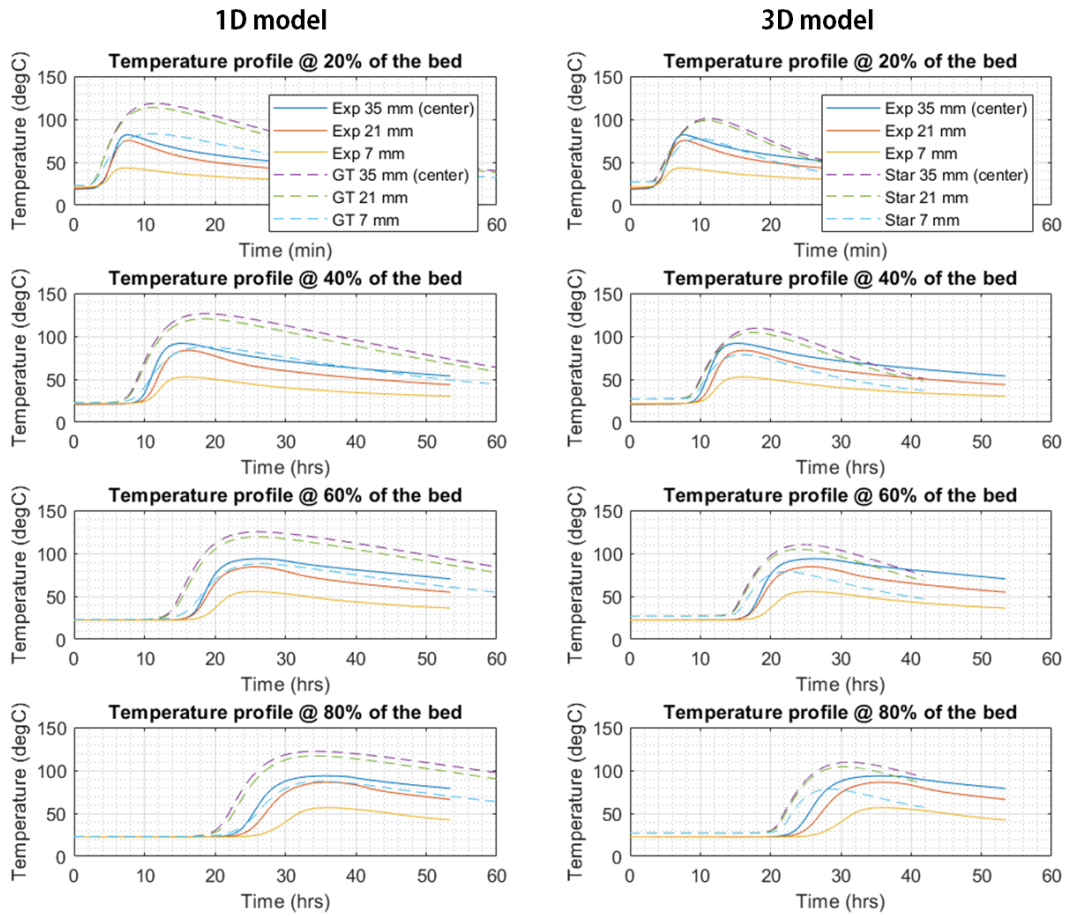


**Figure 4.13:** Comparison of temperature profiles obtained by 1D (left) and 3D (right) simulations for small canister loading process with inlet flowrate of 0.8 L/min (50% n-Butane and 50% Nitrogen).

It should be noted that the 3D model needs further calibration. A decrease in the  $\Delta H$  value and more accurate values of the maximum and dynamic adsorption can improve the results further.

### 4.4.3 Purge gas heating

In the work conducted by Erik Östermark [19], it was shown by simulation work that the addition of heat to the purge flow can enhance the purging process since the desorption process is favoured at higher temperatures. However, the results were not validated by experiments. In this study, the purge gas heating experiments were carried out. Figure 4.14 shows the results of the experiments along with the 1D simulation results.

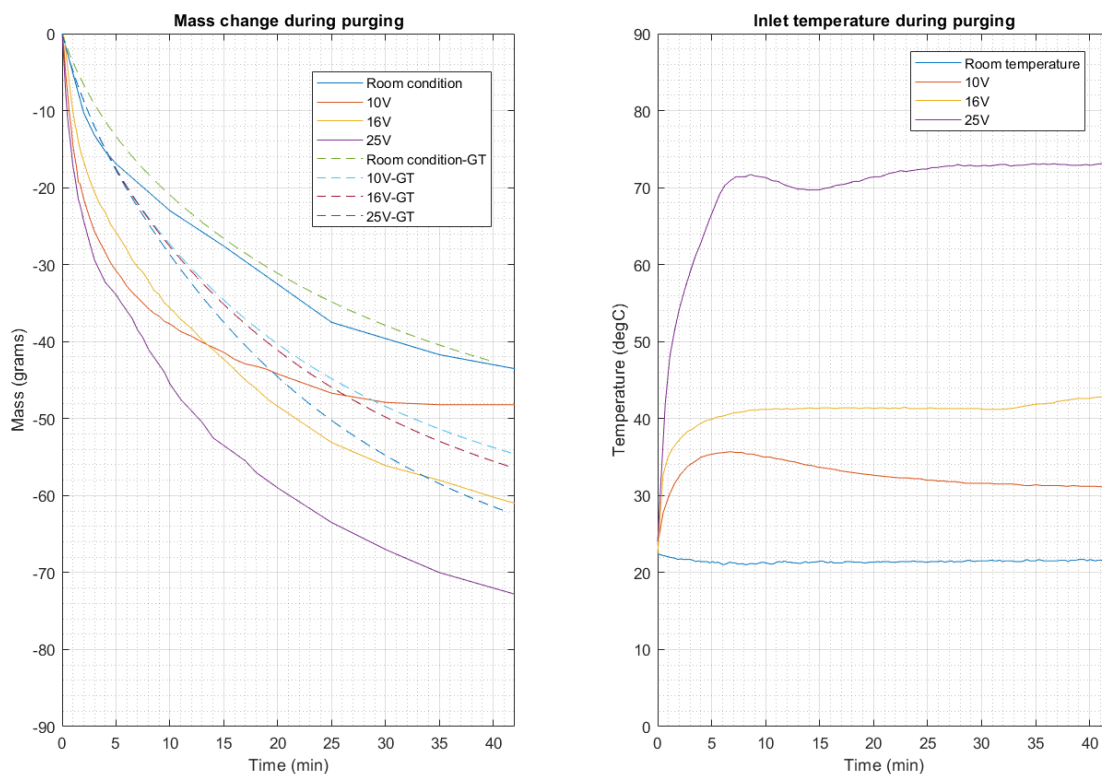


**Figure 4.14:** Left: Comparison of mass loss during purging of small canister between simulation and experimental results. Right: Inlet temperatures for different cases of purge flow heating.

From the graph it can be seen that the case with purge flow inlet at room temperature, about 22°C, shows good agreement between experiment and simulation results. However, at higher inlet temperatures, the mass change profiles start to deviate. Two observations can be made. Firstly, the initial rate of change in mass is smaller in comparison to the experiments and secondly, the amount purged is less than the experimental results. There are several reasons for these variations and they are linked to both shortcomings in the experimental procedure and simulation

method.

During the purge gas heating experiments, it was noted that the mass scale reading was always varying by approximately  $\pm 2-3\text{g}$ . Also, since most of the experimental setup was made of plastic material, there was possible expansion taking place due to high temperature which might have contributed to the change in mass scale readings.

As stated before in section 2.2.4, the values of  $E$ ,  $n$  and  $W_o$  used in this study gave good isotherm fit at  $25^\circ\text{C}$  but at higher temperature of  $100^\circ\text{C}$  the isotherm fitting line started to deviate from experimental values. In figure 2.4 (Right) at low pressure, the model value suggests that the activated carbon is able to hold more n-butane than the experimental results. This means that when purging, the model would release lesser n-butane than the experimental results which might be one of the reasons for the results obtained as shown in figure 4.14.

#### 4.4.4 Altitude variation

In the 1D model in GT-SUITE, there is provision to change altitude in the 'EndEnvironment' template. This feature was utilized to see the effect of altitude variation on the adsorption process inside the small canister. Figure 4.15 shows the results of canister mass gain for different altitudes. All the other parameters such as inlet flowrate and composition are kept constant.

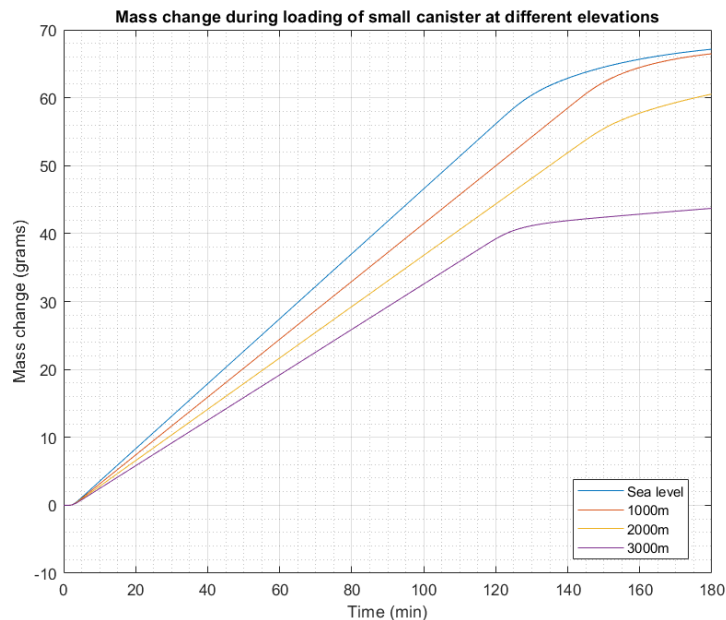


**Figure 4.15:** Effect of altitude variation on the n-butane storage capacity of the small canister (1D model results).

Table 4.2 shows the absolute atmospheric pressure at different altitudes.

**Table 4.2:** Absolute pressure observed in atmosphere at different altitudes (Values taken from GT-SUITE software).

Altitude (m above sea level)	Absolute pressure (bars)
0	1.01325
1000	0.90171
2000	0.80036
3000	0.70846

It can be observed that with an increase in altitude, the capacity of the canister starts to reduce. It can also be seen that the rate of adsorption, given by the slope of the line in the graph, also decreases. The low capacity is due to the fact that at high altitudes, the absolute pressure is lower and the equilibrium coverage starts to reduce because of inverse dependence on absolute pressure. The lower rate of adsorption is also due to the fact that the equilibrium coverage amount is reduced and the term  $[\bar{\theta}^*(t) - \bar{\theta}(t)]$  in equation 2.5 reduces, resulting in a lower value of  $\frac{d\bar{\theta}(t)}{dt}$ .

## 4.5 Canister Insulation

To see the effect of heat loss to the surrounding, the large canister was insulated and the loading and purging experiments were performed again. The results of loading and purging experiments are shown in figure 4.16 and 4.17 respectively.

In the loading experiments, a noticeable increase in temperature inside the carbon bed was observed. The mass change profile was almost the same except for the fact that the breakthrough was achieved 24 minutes earlier for the insulated canister. This was expected since a higher temperature would mean a lower equilibrium coverage and hence a lower capacity for the bed to hold the n-butane. As a result, the breakthrough is achieved earlier. It should be noted that at higher temperature, the rate of adsorption is also reduced but there was no way to check this with the experimental readings taken.

In the purging experiments, the major difference in the temperature profile is observed near the wall where lower temperatures are observed for the insulated canister. Also, the temperature rise after the minimum temperature is reached is also slower for the insulated canister. The recorded mass loss for the insulated canister is also lower in comparison to the uninsulated canister. At lower temperatures, lesser n-butane is released from the activated carbon. Since the heat gain from the surrounding help to keep the temperature up during the purging process, more mass loss is observed for the uninsulated case.

Needless to say, insulation hinders both the loading and purging processes and a wall material with higher conductivity would aid in both these processes.

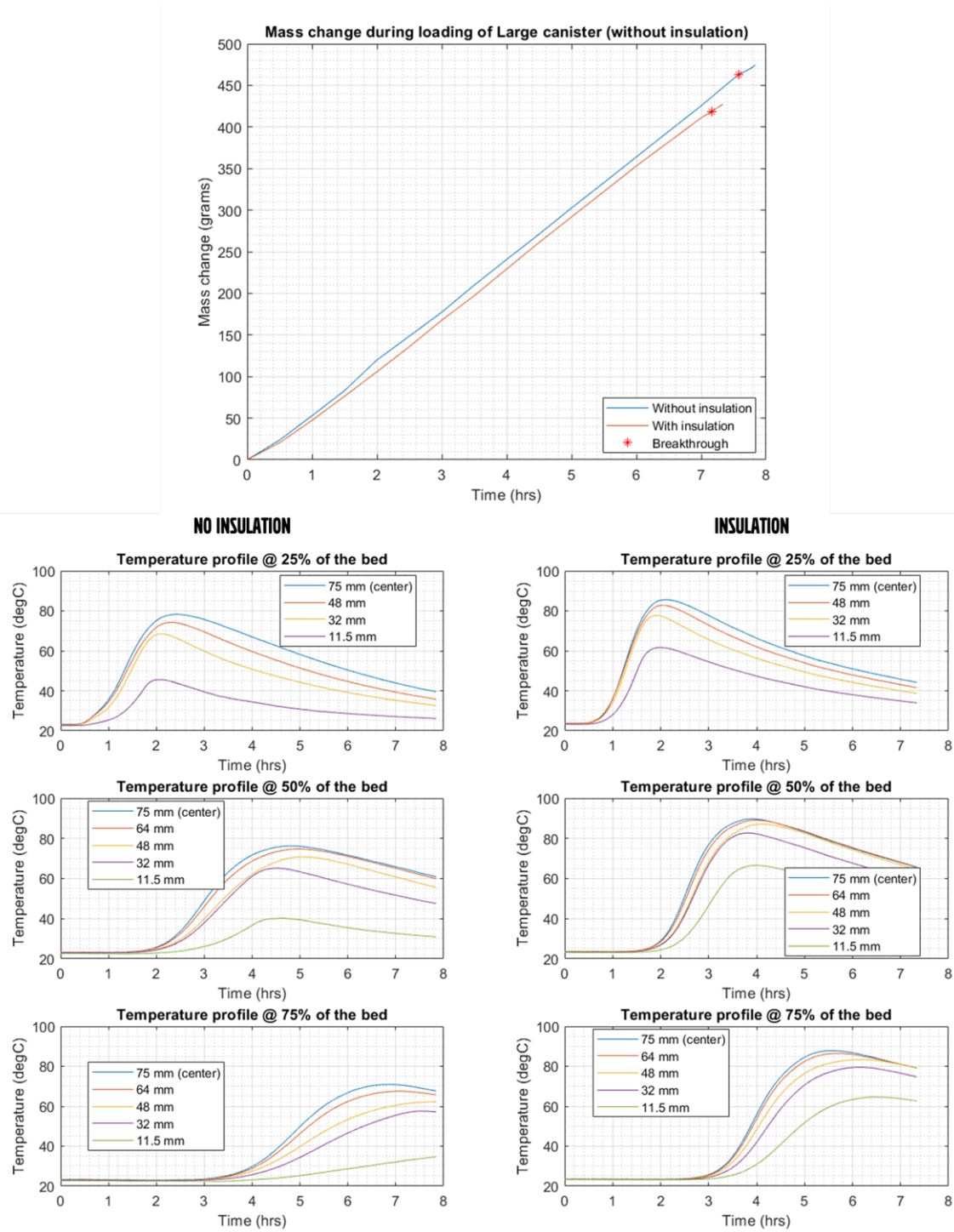


**Figure 4.16:** Mass change and temperature profiles during loading process for insulated and uninsulated canister.

## 4. Results and discussion

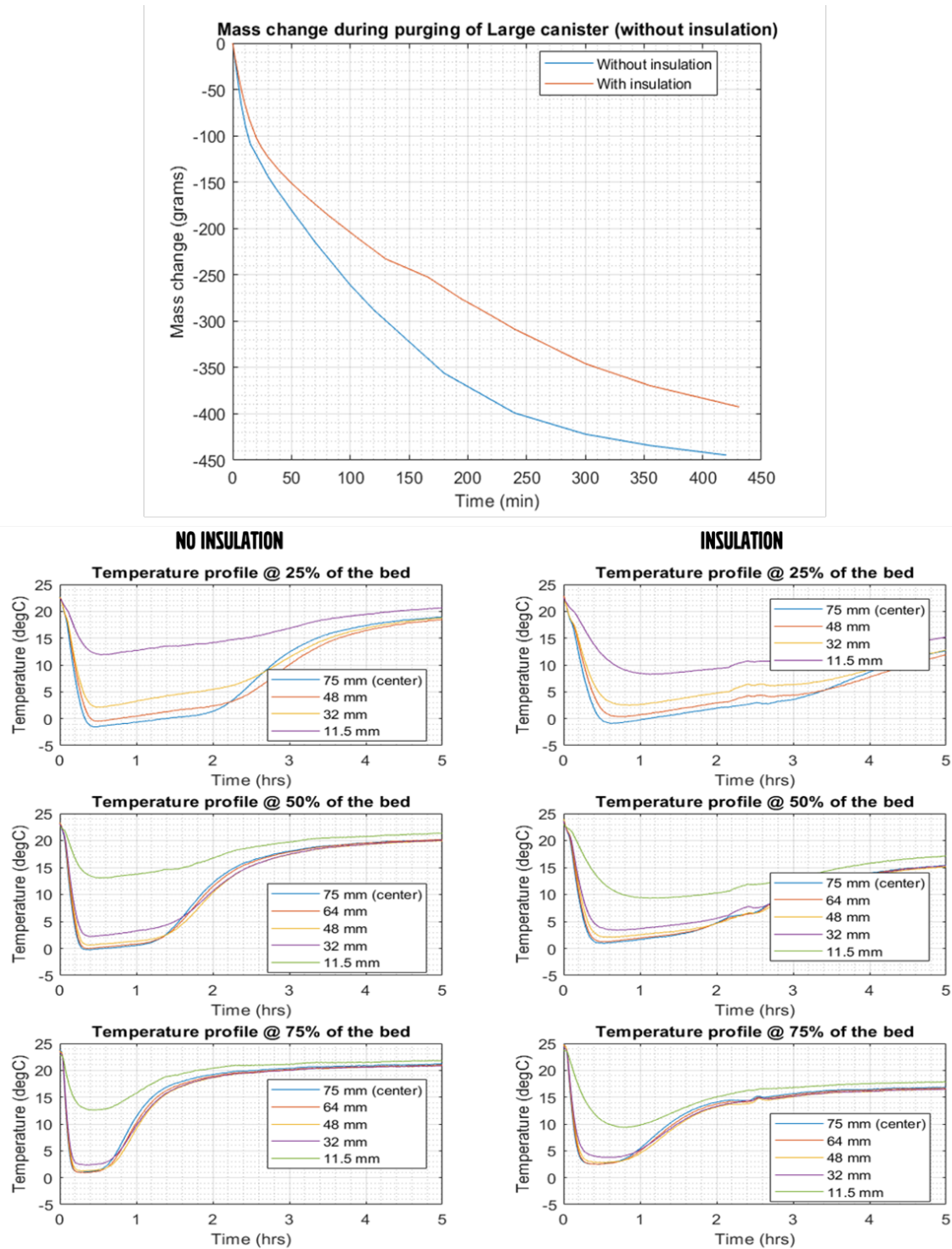


**Figure 4.17:** Mass change and temperature profiles during purging process for insulated and uninsulated canister.

## 4.6 Concentration profiles

An attempt was made to find the concentration profiles inside the carbon bed. For this purpose gas samples were taken from different positions inside the carbon bed at different times. The automotive gas analyzer was used to record the sample readings. The signal profile for one of the loading experiments, carried out on the small canister, is shown in figure 4.18.

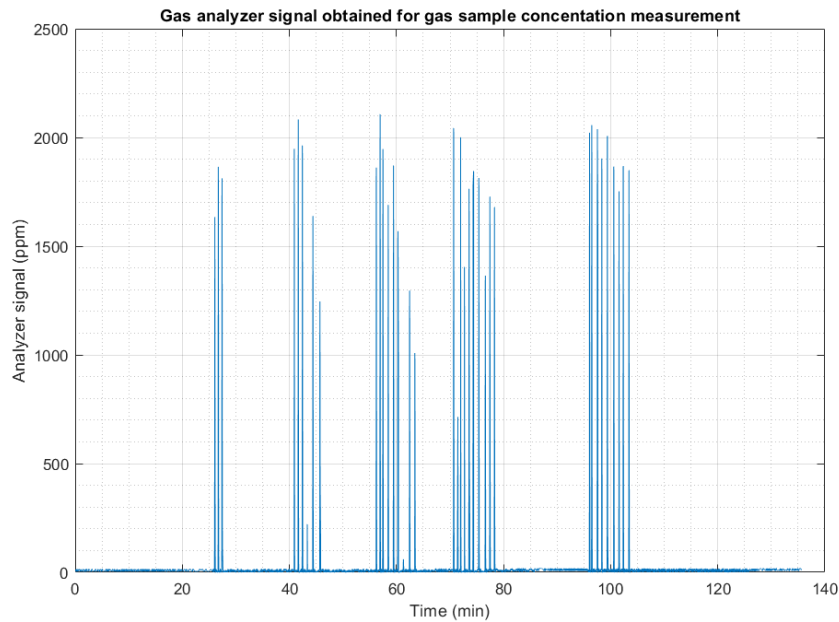


**Figure 4.18:** The signal data received from the automotive emission analyzer for Hydrocarbon concentration in ppmvol for the loading experiment conducted on small canister with total inlet flowrate of 0.4 L/min.

In the above graph, each peak represents a single gas sample. This signal was processed, as mentioned before, to get the actual n-butane concentrations. The actual concentration of n-butane at four different times is shown in figure 4.19. From the graphs it can be seen that the concentration profiles are varying quite alot. Taking the sample reading of 20 mm at 25% bed location as an example, we see from the first 3 points that with time the concentration of n-butane is increasing but the fourth reading is quite low which indicates a drop in concentration. This trend does not seem realistic since with time the bed starts to saturate and the concentration of n-butane at any given point should increase and reach the inlet flow concentration i.e. 50% vol.

There were several shortcomings observed in this method of concentration measurement. Firstly, it was observed that when the analyzer was fed with the same composition gas multiple times, the concentration for each sample was not the same. There was a variation of  $\pm 10\%$  which is quite high. Secondly, it was observed that there was a lag in signal recording sometimes where the analyzer stopped recording

## 4. Results and discussion

for a few seconds. Since the entire signal of a sample lasts for upto 10s, this lag in analyzer recording introduced a very large error in the integration of the signal.

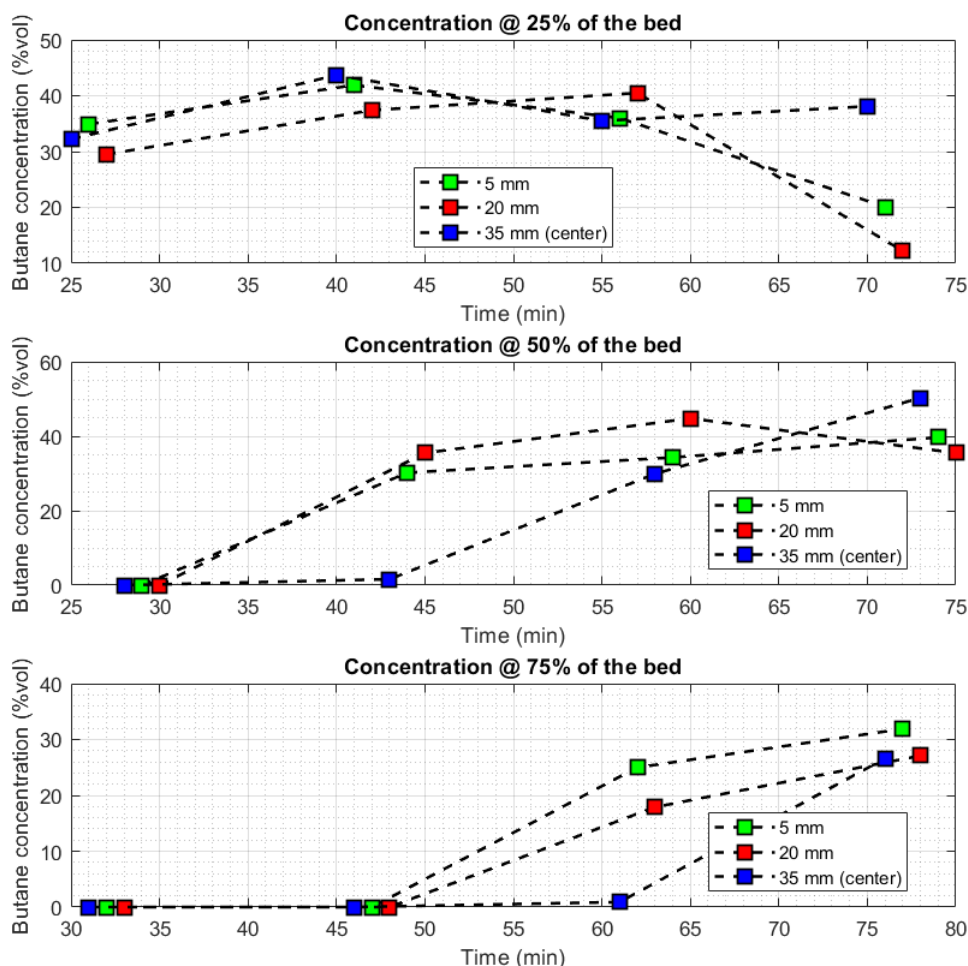


**Figure 4.19:** Loading experiment results of n-Butane concentration at 3 different radial positions inside the small canister with total inlet flowrate of 0.4 L/min.

Due to these inconsistencies and errors, this method of concentration measurement was not a reliable one. It would've been better to use gas chromatography to analyze the gas samples. For this project the chromatograph was not available. Furthermore, the chromatograph takes longer time to analyze a single sample so it was not considered due to very large number of gas samples.

The concentration scene in the 3D model is shown in figure 4.20. It can be seen that the concentration near the wall is slightly higher than the bed center. However, in the absence of reliable concentration profiles from experiments, it is difficult to make a good comparison.

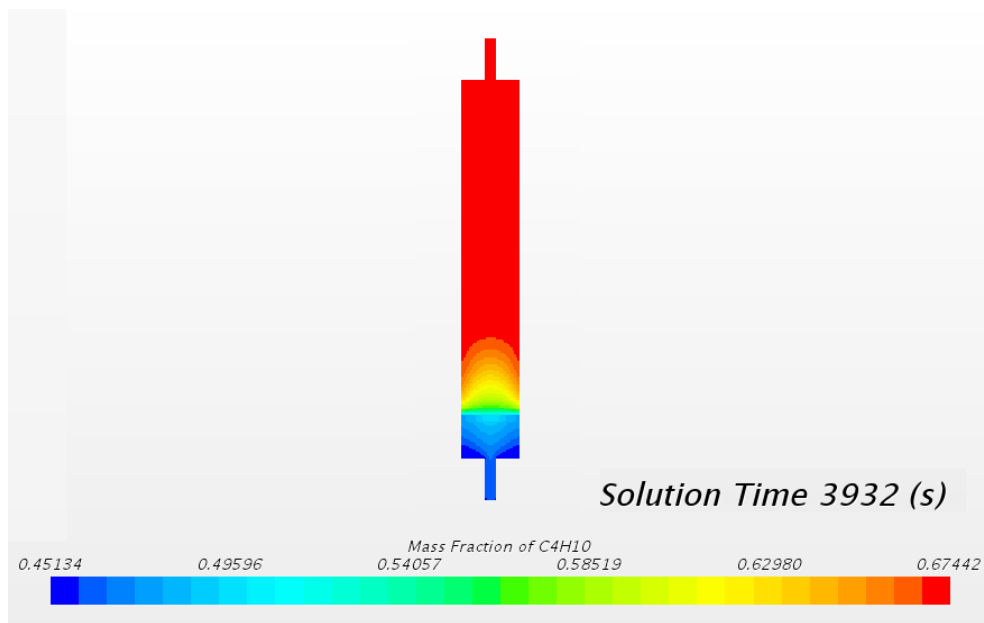


**Figure 4.20:** 3D simulation scene for butane concentration mass fraction in small canister with total inlet flowrate of 0.4 L/min.

The gas sampling experiments for the large canister showed a more clear profile and lesser error in values. Also a larger concentration gradient between points near the wall and bed center was observed. In the large canister, the experimental results were indicating that the breakthrough was occurring at locations near the wall. However, since the large canister was not modelled in 2D or 3D, no comparison of results could be done.



# 5

## Conclusion

A working 1D and 3D model of a carbon canister was developed. The results of both models were validated with experimental data and found to have varying degree of accuracy. The 1D model was able to predict the mass change during loading and purging processes better than the 3D model. On the other hand, the 3D model temperature profiles had better agreement with the experimental profiles than the 1D model. The concentration profiles obtained from the experiments had high degree of error so the 3D model concentration profile results could not be validated. The purge gas heating cases run in 1D model were validated with experimental data and found to be underestimating the mass loss during purging at higher temperatures. The objectives of the thesis were achieved with varying degree of accuracy.

The experimental procedure carried out had several shortcomings. First of all, the method used for measuring n-butane concentration using automotive emission analyzer was found to have very low accuracy. It was found that the analyzer is only good for long term continuous measurement and short sample times give results with very high tolerance. While constructing the canisters, it was a challenge to correctly position the thermocouples and the gas syringe needles and after filling the canister with activated carbon there was no way to check if the positions were correct. During the purge gas heating experiments, it was a challenge to prevent movement of the apparatus and a continuous variation in mass scale was observed, especially at higher temperatures.

The 1D model provides accurate data for mass change during loading and purging. However, for obtaining accurate description of temperature and concentration profiles, 3D model was found to be a better choice. The 3D model developed in this study is not an optimum model since it requires further calibration. Further optimization of tuning parameters can improve the 3D model results further. For 3D model calibration, some additional data of the BAX-1500 activated carbon was needed which was not available so reasonable guesses were made e.g. the maximum adsorption  $n_{max}$  value in 3D model.

Additionally, the effect of altitude variation on the canister loading capacity was seen and it was found that with increasing altitude, the capacity of the canister dropped significantly. An experimental study was done to see the effect of insulation on the canister performance and it was found that having walls with high conductivity aids both the loading and purging processes.



# 6

## Future work

As stated earlier, the 3D model requires further calibration. In this study, the calibration was carried out manually which required a lot of time. An effective calibration method for 3D model should be investigated to reach an optimized result based on tuning parameters.

The experimental procedure for concentration measurement needs improvement. Major issue in the measurement was the low accuracy of the Automotive Emission Analyzer which was giving inconsistent results. A possible remedy to this problem can be the use of chromatography technique instead of the emission analyzer to obtain better concentration results. The results of the simulation should than be validated.

From the obtained results, 3D modelling seems to provide more utility as it can be used to investigate different geometries. A way forward would be to simulate the actual carbon canister along with validation of results based on experiments carried out on actual canister.

Once the 3D model has been validated, the canister geometry can be investigated to find any shortcomings in the current design and improvements can be suggested to modify the canister geometry with better efficiency.



# Bibliography

- [1] Continental-Automotive. Worldwide emission standards and related regulations passenger cars / light and medium duty vehicles, 2017.
- [2] Martyn V. Twigg. Progress and future challenges in controlling automotive exhaust gas emissions. *Applied Catalysis B: Environmental*, 70(1):2 – 15, 2007. Papers presented at the 4th International Conference on Environmental Catalysis (4th ICEC)Heidelberg, Germany, June 05 – 08, 2005.
- [3] Roger Atkinson and Janet Arey. Atmospheric degradation of volatile organic compounds. *Chemical Reviews*, 103(12):4605–4638, 2003. PMID: 14664626.
- [4] In Kwang Yoo, Devesh Upadhyay, and Giorgio Rizzoni. A control-oriented carbon canister model. *SAE Transactions*, 108:2133–2142, 1999.
- [5] Manufacturers of Emission Controls Association et al. Evaporative emission control technologies for gasoline powered vehicles, 2010.
- [6] Uwe Mohr. Activated carbon canisters for automobiles. *Filtration and Separation*, 34, 12 1997.
- [7] Roger S Williams and C Reid Clontz. Impact and control of canister bleed emissions. *SAE Transactions*, pages 579–587, 2001.
- [8] Chongzhi Zhong, Tieqiang Fu, Chunbei Dai, Taiyu Zhang, Ke Wu, and Wangwen Gu. The influence on working performance of the canister cavity design. Technical report, SAE Technical Paper, 2017.
- [9] Motoyuki Suzuki. *Fundamentals of adsorption*, volume 80. Elsevier, 1993.
- [10] AS Negi and SC Anand. *A textbook of physical chemistry*. New Age International, 1985.
- [11] Junior D Seader, Ernest J Henley, and D Keith Roper. Separation process principles. 1998.
- [12] WJ Thomas and B Crittenden. Fundamentals of adsorption equilibria. *Adsorption Technology & Design*, pages 31–65, 1998.
- [13] Erik Möller. *Modelling and Simulation of an Activated Carbon Canister*. Chalmers University of Technology, 2016.
- [14] Douglas M Ruthven. *Principles of adsorption and adsorption processes*. John Wiley & Sons, 1984.
- [15] Emmanuel Fiani, L Perier-Cambry, and Gérard Thomas. Non-isothermal modelling of hydrocarbon adsorption on a granulated active carbon. *Journal of thermal analysis and calorimetry*, 60(2):557–570, 2000.
- [16] S Sircar and JR Hufton. Why does the linear driving force model for adsorption kinetics work? *Adsorption*, 6(2):137–147, 2000.
- [17] George Wm Thomson. The antoine equation for vapor-pressure data. *Chemical reviews*, 38(1):1–39, 1946.

- [18] Peter J Linstrom and William G Mallard. The nist chemistry webbook: A chemical data resource on the internet. *Journal of Chemical & Engineering Data*, 46(5):1059–1063, 2001.
- [19] Erik Östermark. *Modelling of a Purge Heated Carbon Canister Using CFD*. Chalmers University of Technology, 2018.
- [20] Gamma Technologies LLC. *GT-SUITE V2017 Flow Theory Manual*. 2018.
- [21] Gamma Technologies LLC. *GT-SUITE V2017 Aftertreatment Manual*. 2018.
- [22] Siemens CD-adapco. *Star-CCM+ User Guide*. 2018.
- [23] Bengt Andersson, Ronnie Andersson, Love Håkansson, Mikael Mortensen, Rahman Sudiyo, and Berend Van Wachem. *Computational fluid dynamics for engineers*. Cambridge University Press, 2011.
- [24] Feng Ye, Jinsheng Xiao, Binxiang Hu, Pierre Benard, and Richard Chahine. Implementation for model of adsorptive hydrogen storage using udf in fluent. *Physics Procedia*, 24:793–800, 2012.